

RESEARCH ARTICLE

The Eurasian Arctic Ocean along the MOSAiC drift in 2019–2020: An interdisciplinary perspective on physical properties and processes

Kirstin Schulz^{1,2,*} , Zoe Koenig^{3,4,5}, Morven Muilwijk⁴, Dorothea Bauch^{6,7}, Clara J. M. Hoppe², Elise S. Droste^{2,8}, Mario Hoppmann², Emelia J. Chamberlain^{9,10}, Georgi Laukert^{10,11}, Tim Stanton¹², Alejandra Quintanilla-Zurita², Ilker Fer⁵, Céline Heuzé¹³, Salar Karam¹³, Sebastian Mieruch-Schnüller², Till M. Baumann^{5,14}, Myriel Vredenborg², Sandra Tippenhauer², and Mats A. Granskog⁴

The Multidisciplinary drifting Observatory for the Study of Arctic Climate (MOSAiC, 2019–2020), a year-long drift with the Arctic sea ice, has provided the scientific community with an unprecedented, multidisciplinary dataset from the Eurasian Arctic Ocean, covering high atmosphere to deep ocean across all seasons. However, the heterogeneity of data and the superposition of spatial and temporal variability, intrinsic to a drift campaign, complicate the interpretation of observations. In this study, we have compiled a quality-controlled physical hydrographic dataset with best spatio-temporal coverage and derived core parameters, including the mixed layer depth, heat fluxes over key layers, and friction velocity. We provide a comprehensive and accessible overview of the ocean conditions encountered along the MOSAiC drift, discuss their interdisciplinary implications, and compare common ocean climatologies to these new data. Our results indicate that, for the most part, ocean variability was dominated by regional rather than seasonal signals, carrying potentially strong implications for ocean biogeochemistry, ecology, sea ice, and even atmospheric conditions. Near-surface ocean properties were strongly influenced by the relative position of sampling, within or outside the river-water influenced Transpolar Drift, and seasonal warming and meltwater input. Ventilation down to the Atlantic Water layer in the Nansen Basin allowed for a stronger connectivity between subsurface heat and the sea ice and surface ocean via elevated upward heat fluxes. The Yermak Plateau and Fram Strait regions were characterized by heterogeneous water mass distributions, energetic ocean currents, and stronger lateral gradients in surface water properties in frontal regions. Together with the presented results and core parameters, we offer context for interdisciplinary research, fostering an improved understanding of the complex, coupled Arctic System.

Keywords: Arctic Ocean, MOSAiC, Spatial variability, Hydrography, Transpolar Drift, Heat fluxes

1. Introduction

To a large extent, the Arctic Ocean has been historically inaccessible due to its perennial ice cover, resulting in

limited data availability, particularly during winter. With global warming triggering rapid transformations in the Arctic (Rantanen et al., 2022), a better understanding of

¹Oden Institute for Computational Engineering and Sciences, The University of Texas at Austin, Austin, TX, USA

⁹Scripps Institution of Oceanography, University of California, San Diego, CA, USA

²Alfred Wegener Institute Helmholtz Centre for Polar and Marine Research, Bremerhaven, Germany

¹⁰Woods Hole Oceanographic Institution, Woods Hole, MA, USA

³UiT The Arctic University of Norway, Tromsø, Norway

¹¹School of Earth Sciences, University of Bristol, Bristol, UK

⁴Norwegian Polar Institute, Fram Centre, Tromsø, Norway

¹²Oceanography Department, Naval Postgraduate School, Monterey, CA, USA

⁵Geophysical Institute, University of Bergen, Bjerknes Centre for Climate Research, Bergen, Norway

¹³Department of Earth Sciences, University of Gothenburg, Gothenburg, Sweden

⁶Leibniz-Laboratory, University of Kiel (CAU), Kiel, Germany

¹⁴Institute of Marine Research, Bergen, Norway

⁷GEOMAR Helmholtz Centre for Ocean Research, Kiel, Germany

* Corresponding author:
Email: kiki.schulz@utexas.edu

⁸School of Environmental Sciences, University of East Anglia, Norwich, UK

processes in the Arctic Ocean and its role in the coupled climate system is urgently needed to accurately predict the effects of a changing climate. Ongoing changes in the Arctic Ocean include declining sea ice cover and longer open water seasons (e.g., Stroeve et al., 2008; Kwok, 2018; Kim et al., 2023), Atlantification, that is, the progression of conditions typical for the North Atlantic farther into the Arctic Ocean (Polyakov et al., 2017), a weakening upper ocean stratification, enhanced vertical mixing and transport (Polyakov et al., 2020a; Polyakov et al., 2020b; Schulz et al., 2022a), increased primary productivity (Arrigo and van Dijken, 2015), and changes in the Arctic ecosystem composition (Gordó-Vilaseca et al., 2023). These changes are observed primarily in the Eastern Arctic, while conditions in the Western Arctic exhibit less clear patterns, for example, no conclusive evidence of increased mixing (Dosser et al., 2021; Fine and Cole, 2022), or even show opposite trends, for example, increased stratification by freshwater accumulation in the Beaufort Gyre (Timmermans and Toole, 2023).

The Multidisciplinary drifting Observatory for the Study of Arctic Climate (MOSAiC) was a year-long (2019–2020) drift campaign with the aim to improve our process-level understanding of the coupled Arctic System (Nicolaus et al., 2022; Rabe et al., 2022; Shupe et al., 2022; Fong et al., 2023). A large number of interdisciplinary efforts in MOSAiC involved physical oceanography parameters, such as ocean temperature and salinity or current velocity. Examples include efforts to calculate the solubility of gases, to determine the origin of water masses that transport tracers and organisms, to quantify the contribution of oceanic heat to sea ice formation and melting, and to constrain the variability in ice-nucleating particles of marine origin. In addition, the modeling community requires updated oceanic boundary conditions and core parameters for model validation (Heuzé et al., 2023b), while climatological datasets, which are often crucial components in modeling frameworks, need ground-truthing to current conditions. However, the diversity of oceanographic equipment used during MOSAiC and the resulting scattered datasets at various levels of processing and documentation hinder easy access to and utilization of these data, especially for non-physical oceanographers and scientists not involved in the field campaign. In addition, the design of MOSAiC as a drifting platform complicates the interpretation of oceanographic measurements. Superimposed on the annual cycle is the regionality along the more than 3500 km long drift track across the Eurasian basin (**Figure 1a**; Rabe et al., 2022). These challenges might lead to an inconsistent usage and interpretation of the oceanographic data and hinder the inter-comparability of individual studies in the future.

In this study, we have compiled an accessible and quality-controlled dataset of hydrographic profiles at the highest possible temporal resolution along the drift and provide derived core parameters (Schulz et al., 2023b), including an interactive data interface (Mieruch, 2023) in the online Ocean Data View webODV (Mieruch and Schlitzer, 2023), which can be used consistently in future disciplinary and interdisciplinary studies. Based on this

dataset, we present a comprehensive overview of ocean conditions during the MOSAiC drift, discuss their effect on the coupled system and, to the extent possible, discriminate between spatial and temporal signals. This description of the state of the Eurasian Arctic Ocean in 2019–2020 and the comparison of commonly used climatological datasets to these modern data will also aid the evaluation of ocean models.

The structure of this article is as follows. In Section 2, we provide a brief overview of the methods and instrumentation used in this study (more detailed information is available in Text S1). Section 3 describes the geography along the drift track of MOSAiC, and in Section 4, we summarize the water column structure and water mass distribution. Section 5 then focuses on dynamic features, such as surface and tidal current variability and eddies. Parameters related to ocean mixing, such as the vertical diffusivity and heat fluxes, are presented in Section 6. In Section 7, we compare MOSAiC results to existing climatologies. In Section 8, we contextualize the MOSAiC data by comparing them to previous findings and discuss the implications of these results for other scientific disciplines. Finally, Section 9 summarizes the main findings and concludes the article.

2. Methods and instrumentation

The MOSAiC drift started in September 2019, using the icebreaker RV *Polarstern* (Knust, 2017) as a drifting platform frozen into the Arctic sea ice, with measurements conducted from the same ice floe and surrounding sites during five cruise legs. On-site sampling was interrupted from May 15 to June 27, 2020, due to the unavailability of a second icebreaker during the COVID-19 pandemic to perform personnel exchange and resupply, but resumed on the same floe. At the end of July, the floe disintegrated in the marginal ice zone in Fram Strait; after relocation north, a second floe was chosen close to the previous drift track to sample the freeze-up period. In the following, we briefly summarize the different datasets and methods used in this study. More details can be found in Text S1, and an overview of the sampling locations is presented in Rabe et al. (2022).

We obtained water depths from three different sources: the *Polarstern* echosounder, the combined altimeter and depth readings from the deep casts of the ship-based conductivity-temperature-depth (CTD) profiling system, and the International Bathymetric Chart of the Arctic Ocean (IBCAO) v4.2 bathymetric dataset (Jakobsson et al., 2020). Drift track and speed were obtained from the *Polarstern* navigation records and complemented with data from a GPS buoy (“CO1”) that remained on the floe when sampling was interrupted in spring. From the drift velocity, we calculated the ice friction velocity u_* based on the Rossby similarity (see Text S1), as done in Kawaguchi et al. (2022).

In total, a set of 2,434 vertical temperature and salinity profiles were compiled, including data from the micro-structure profiler (MSS) operated at Ocean City, that is, a sampling site in the Central Observatory (CO) on the main floe (1,665 profiles, 0–350 m; Schulz et al.,

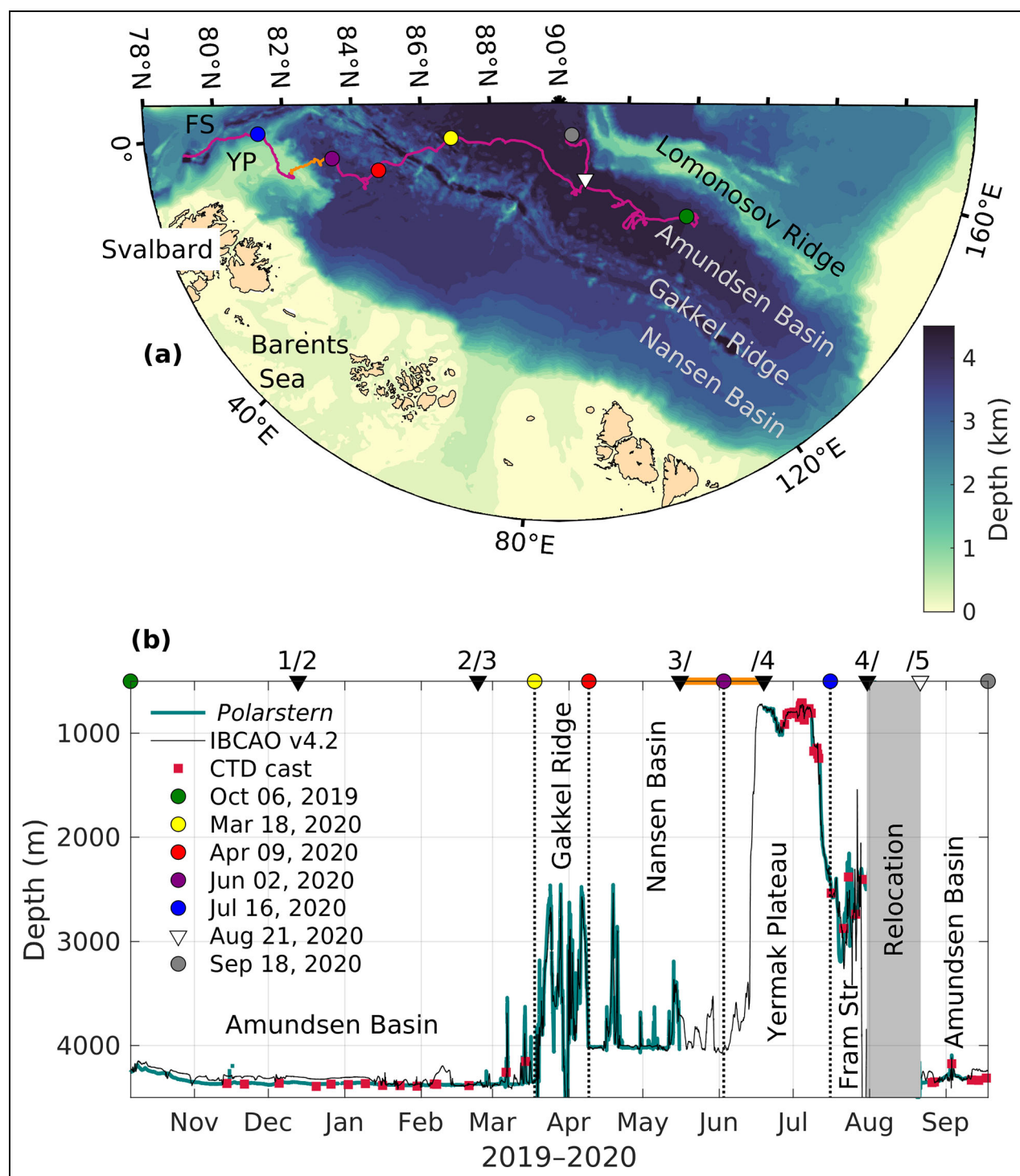


Figure 1. Bathymetry along the drift track. (a) Bathymetric map of the Arctic Ocean with drift track (violet from *Polarstern*, orange from positioning buoy “CO1” between Legs 3 and 4) indicated; (b) bathymetry along the drift track from the *Polarstern* echosounder (teal), International Bathymetric Chart of the Arctic Ocean (IBCAO v4.2) dataset (black) and the deep conductivity, temperature, depth (CTD) casts (red squares). For better orientation, landmarks of the drift and the start and end of the individual legs are indicated with colored dots and triangles in both panels. The orange line in (b) indicates the time period when the floe was left uncrewed.

2023c), the Ocean City CTD (121 profiles, down to maximum 1000 m; Tippenhauer et al., 2023a) and the *Polarstern* CTD (134 profiles, excluding those during transit; Tippenhauer et al., 2023b). During the drift interruption and on days without any MSS or CTD casts, we used profiles from the ice-tethered profilers ITP94 and ITP111 (428

profiles, down to 1000 m depth; Toole and Krishfield, 2016) and daily mean data at five discrete depths (10 m, 25 m, 50 m, 75 m, 100 m) from a CTD chain on Pacific Gyre buoy 2019O4 (86 days; Hoppmann et al., 2022), all deployed near the CO at the start of the drift. Data from all instruments were converted to conservative temperature

Θ ($^{\circ}$ C) and absolute salinity S_A (g kg^{-1}), quality-controlled and cross-calibrated where necessary (see Text S1). Temperature readings from the *Polarstern* thermosalinograph are excluded here, as they were found to be unreliable (Figure S1). We recommend not using these data in future analyses.

We calculated the mixed layer depth, that is, the vertical extent of the surface layer with uniform temperature, salinity, and hence density, as the first depth where the potential density anomaly σ_0 increases by $\Delta\sigma_0 > 0.04 \text{ kg m}^{-3}$ compared to the surface (4–10 m) mean value (or, 0.06 kg m^{-3} if the increase in density at the base of the mixed layer was more gradual; see Text S1). We have omitted giving mixed layer depth estimates in the presence of strong upper (0–10 m) ocean stratification (i.e., when there is no classical mixed layer, conditions frequently found during melt season), or when mixed layer depth estimates based on different density thresholds (0.04 – 0.08 kg m^{-3}) were very variable (i.e., the base of the mixed layer was not well defined). Surface salinity and temperature were calculated as the average over 4–10 m depth (to exclude sampling points within an under-ice meltwater lens in spring for the MSS), and the corresponding freezing point temperature was calculated based on the TEOS-10 set of equations (McDougall and Barker, 2011). Additionally, to better identify the surface water composition and origin, we calculated the surface layer (0–15 m) river water fraction based on an end-member analysis using $\delta^{18}\text{O}$ isotope and salinity measurements (Text S1; Bauch et al., 2011) and colored dissolved organic matter (CDOM, an indicator for riverine water) fluorescence from ITP94 (before relocation only; e.g., Granskog et al., 2007; Gonçalves-Araujo et al., 2016; Stedmon et al., 2021b). We characterized water masses and layers as follows:

- The surface mixed layer (ML) from the surface to the base of the ML as explained above and in Text S1;
- The halocline layer (HAL) from the base of the ML to $R = \frac{\alpha\Delta\theta}{\beta\Delta S} = 0.05$, where α is the thermal expansion and β is the haline contraction coefficient, following Bourgain and Gascard (2011);
- The Atlantic Water thermocline (THERM) from the first depth below the halocline where the temperature exceeds 0.8 times the minimum temperature in the halocline to the first depth where the temperature exceeds 0.8 times the maximum temperature of the Atlantic Water layer, as defined in Schulz et al. (2021);
- Arctic Atlantic Water (AAW) as the conservative temperature range $0^{\circ}\text{C} < \Theta < 2^{\circ}\text{C}$ (Korhonen et al., 2013);
- Atlantic Water (AW) with conservative temperature $\Theta > 2^{\circ}\text{C}$ (Rudels, 2012);
- Upper Polar Deep Water (UPDW) from the first depth when temperatures fall below $\Theta = 0^{\circ}\text{C}$, down to $\sigma_{0.5} = 30.444 \text{ kg m}^{-3}$, the potential density referenced at 500 m depth (Rudels, 2009);
- Eurasian Basin Deep Water (EBDW) between $\sigma_{0.5} = 30.444 \text{ kg m}^{-3}$ and $\sigma_1 = 37.46 \text{ kg m}^{-3}$

(Smethie et al., 1988). σ_1 refers to the potential density referenced at 1000 m depth;

- Canadian Basin Deep Water (CBDW) with the same range as EBDW, but with $\Theta > -0.6^{\circ}\text{C}$ and absolute salinity $S_A > 35.083 \text{ g kg}^{-1}$ following Rudels (2009), with the salinity threshold converted from practical salinity of 34.915 in Rudels (2009) at 1500 m depth;
- Eurasian Basin Bottom Water (EBBW) from $\sigma_1 = 37.46 \text{ kg m}^{-3}$ to the sea floor (Smethie et al., 1988);
- In the Yermak Plateau and Fram Strait regions: Arctic Intermediate Water (AIW) in the same range as UDW ($\Theta = 0^{\circ}\text{C}$ to $\sigma_{0.5} = 30.444 \text{ kg m}^{-3}$) following Meyer et al. (2017b);
- In the Yermak Plateau and Fram Strait regions: Nordic Sea Deep Water (NSDW) from $\sigma_{0.5} = 30.444 \text{ kg m}^{-3}$ to the sea floor (Meyer et al., 2017b).

Current velocity profiles (approximately 20–400 m depth) obtained with a 75 kHz acoustic Doppler current profiler (ADCP; Baumann et al., 2021) were used to calculate depth-averaged surface layer (14–30 m) and tidal (whole water depth) currents of different frequencies (see Meyer et al., 2017b and Text S1 for more details on the methodology) and to identify eddies visually. Tidal velocities were then compared to data from the Arctic Ocean Tidal Inverse Model AOTIM5 (Erofeeva and Egbert, 2020).

Turbulent mixing parameters presented here are based on the dissipation rate of turbulent kinetic energy ε , measured with the MSS (Schulz et al., 2022b). The value ε describes how much small (0.1–1 m) scale turbulent kinetic energy (“turbulence”) is present to mix the water column. From ε , we calculated the depth of the surface active mixing layer, that is, the depth range where turbulence is elevated due to friction at the ocean-sea ice interface ($\varepsilon \geq 5 \times 10^{-9} \text{ W kg}^{-1}$). From ε and the local stratification, we calculated the turbulent diffusivity K_z along each profile, as described in Bouffard and Boegman (2013). This method takes into account how K_z scales in different energetic regimes, that is, in the presence of high or low turbulence and strong or weak stratification. Spatio-temporal averages in different regions or over certain vertical layers were obtained using the maximum likelihood estimator (MLE; Baker and Gibson, 1987) and heat fluxes over the halocline and thermocline (Section 2) were calculated following Schulz et al. (2021). In addition, eddy-correlation-based heat fluxes at 3 m depth were measured with an Autonomous Ocean Flux buoy at a distance of 15–25 km from *Polarstern* (Stanton et al., 2012; Stanton and Shaw, 2023).

We compare four typical Arctic Ocean climatological datasets and two commonly used state estimates (i.e., models constrained with observational data to minimize the misfit to these observations), listed in **Table 1**, to the MOSAiC data. These data products cover different time periods, contain different types of data from various sources and are produced using distinct methods and interpolation procedures (see Text S1 for details).

3. Geography along the drift track

The Arctic Ocean is a semi-enclosed basin, connected to the Atlantic Ocean via Fram Strait between Svalbard and

Table 1. Climatologies and state estimates (*italics*) of temperature and salinity used for comparison with the MOSAiC observations (Section 7)

Dataset	Reference	Vertical Layers	Temporal Coverage
PHC3	Steele et al. (2001)	24	1948–1997
WOA18	Locarnini et al. (2018); Zweng et al. (2018)	57	1955–2017
MIMOC	Schmidtko et al. (2013)	81	1970–2011
WOA23	Boyer et al. (2018)	57	1991–2020
ASTE	Nguyen et al. (2021)	50	2002–2017
ECCOv4	Forget et al. (2015)	50	1992–2015

Greenland and the Barents Sea and to the Pacific via the Bering Strait between Russia and Alaska. Surrounded by wide shelf seas, the deep Arctic basin is separated by the Lomonosov Ridge, which reaches from the Siberian shelf to the Canadian shelf, into the Amerasian and Eurasian basins. The Eurasian Basin is further divided into the Amundsen Basin and the Nansen Basin by the Gakkel Ridge (**Figure 1a**). The shallow Yermak Plateau extends northwards from the continental shelf on which the Svalbard archipelago is located, with the Nansen Basin on its eastern side and Fram Strait on its western side. These geographic divides have a large impact on Arctic Ocean circulation patterns and hence on the water column structure in the different regions. When interpreting the results from a drift campaign such as MOSAiC, regional gradients have to be taken into account.

The MOSAiC drift started in October 2019 in the 4400 m deep Amundsen Basin (green dot in **Figure 1**) and progressed parallel to the Gakkel Ridge within the basin over virtually flat bottom topography for around 5 months. The drift then crossed the rough topography of the Gakkel Ridge over a 3-week time period between March 18 and April 9, 2020 (yellow to red dot in **Figure 1**), and crossed the Nansen Basin. At the beginning of June, the drift reached the shallow Yermak Plateau (local depth approximately 800 m; purple dot in **Figure 1**) northwest of Svalbard. After crossing the plateau from east to west, the floe entered the deeper waters and complex topography of Fram Strait on July 16 (blue dot in **Figure 1**) and drifted south, until the floe eventually broke up in the marginal ice zone. After a relocation closer to the North Pole, in the vicinity of the previous drift track (white triangle in **Figure 1**), measurements were resumed on a second floe in the Amundsen Basin. This time, the drift was directed northwards, parallel to the Lomonosov Ridge, until the expedition ended on September 20, 2020.

Compared to the water depth measurements from MOSAiC, we found that the bathymetric data from IBCAO v4.2 perform well in the basins and for the Gakkel Ridge and Yermak Plateau region, but agree less well with the highly variable bottom depth in Fram Strait. In the following, we use the bathymetric data from IBCAO and any basin averages (e.g., of temperature and salinity profiles) refer to averages over the regions indicated above and in **Figure 1b**, with a discrimination between conditions in

the Amundsen Basin during winter (first part of the drift) and during summer (last part of the drift).

4. Water column structure and variability

In the following sections, we provide a short general overview of the water masses of the Eurasian Arctic Ocean and their formation and characteristics (Section 4.1). We then elaborate on the observed variability of the near-surface waters (Section 4.2), the Atlantic Water layer (Section 4.3) and the deep water masses (Section 4.4) during the MOSAiC drift.

4.1. Water masses in the Arctic Ocean

Large amounts of terrestrial freshwater (and other material) enter the Arctic Ocean from Siberia and are advected toward Fram Strait together with sea ice formed on the Siberian shelves transported via the Transpolar Drift (e.g., Mysak, 2001; Karcher et al., 2012; Rudels, 2012; Charette et al., 2020). Both the transport of freshwater and sea ice across the Arctic Ocean are often referred to as the “Transpolar Drift.” While both transport patterns are qualitatively similar, the exact transport pathway and the velocities of sea ice and river water-rich surface water differ (see Section 5). In this study, Transpolar Drift refers to the transport of relatively fresh, river water-rich surface water from Siberian regions toward Fram Strait unless specified otherwise.

The surface waters within the Transpolar Drift are characterized by high concentrations of dissolved organic carbon (DOC) and various lithogenic elements and may carry organisms originating from the coastal and shelf zones (Krumpen et al., 2019; Charette et al., 2020). Paffrath et al. (2021) showed, based on lithogenic provenance tracers, that most of the freshwater encountered in the Eurasian Arctic Ocean is derived from the Lena, Yenisei, and Ob rivers, whose contributions do not fully mix and form distinct freshwater domains within the Transpolar Drift. The high nutrient loads in these terrestrial waters is partially utilized on the wide Siberian shelves (Laukert et al., 2022), and their role for primary production at the pan-Arctic scale is still not entirely clear (Fouest et al., 2013; Terhaar et al., 2021; Gibson et al., 2022). Mixed with ambient waters, this land-runoff forms a relatively fresh surface layer uniform in temperature and salinity: the polar mixed layer (ML; gray in **Figure 2c** of the MOSAiC data). This surface layer is bound by a pycnocline, that is, a sharp

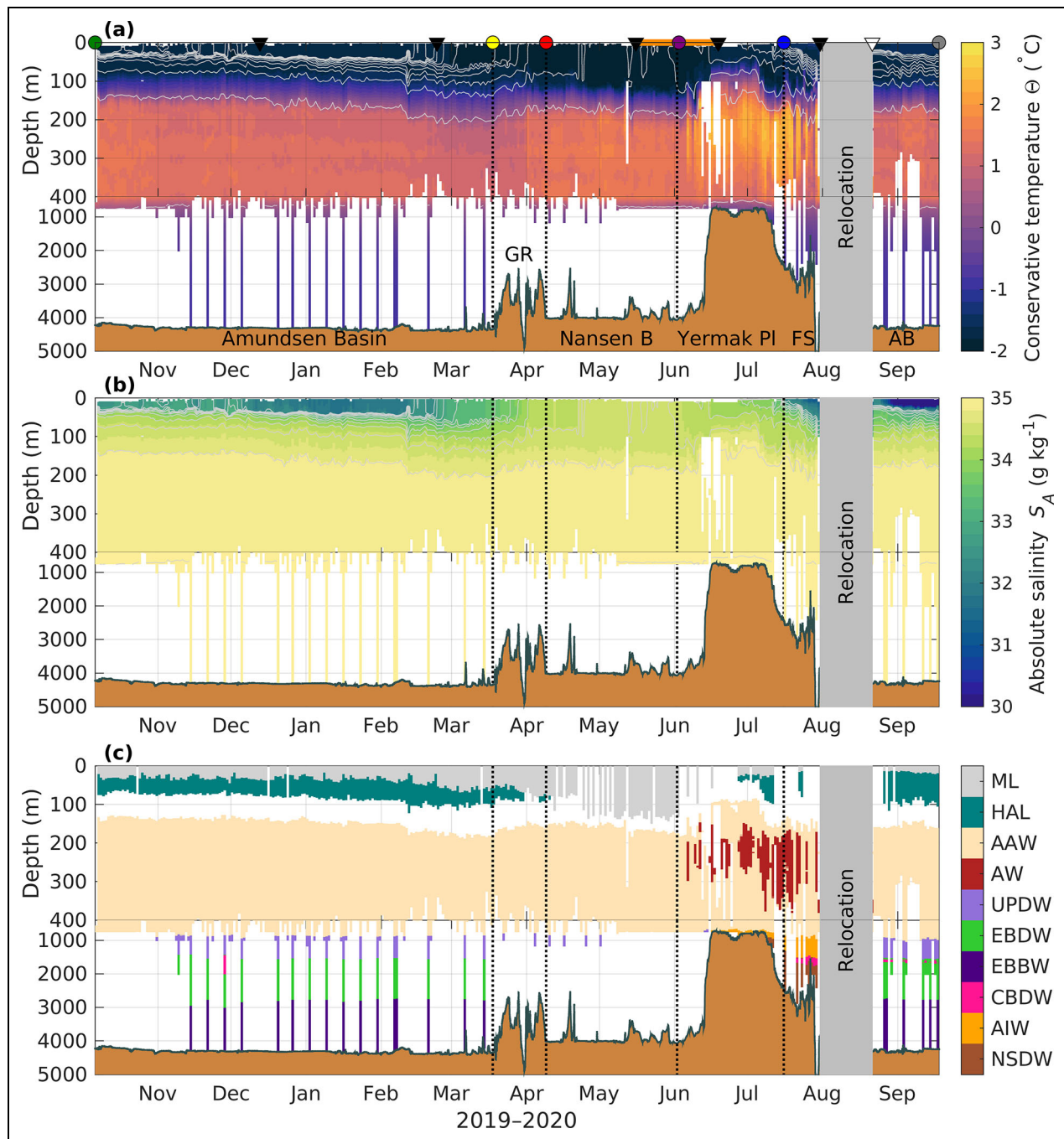


Figure 2. Water mass distribution along the drift. (a) Conservative temperature ($^{\circ}\text{C}$), (b) absolute salinity (g kg^{-1}), and (c) water mass distribution along the drift, based on the composite dataset presented in this study. In (a–c), topographic regions are shown (in brown), including the Amundsen Basin (AB), Gakkel Ridge (GR), Nansen Basin (B), Yermak Plateau (Pl), and Fram Strait (FS); the white regions have no data coverage. Gray lines in (a) and (b) indicate isopycnals with a spacing of 0.2 kg m^{-3} . The color bar in (c) indicates the mixed layer (ML), halocline (HAL), Arctic Atlantic Water (AAW), Atlantic Water (AW), Upper Polar Deep Water (UPDW), Eurasian Basin Deep Water (EBDW), Eurasian Basin Bottom Water (EBBW), Canadian Basin Deep Water (CBDW), Arctic Intermediate Water (AIW), and Nordic Sea Deep Water (NSDW). Data gaps in June are caused by ice-tethered profiler (ITP) data not covering the whole water column. Note that the y-axis is nonlinear, zoomed in the upper 400 m. In (a), triangles indicate the start and end of the legs; dots and vertical dotted lines, the geographical markers; and the orange line, the uncrewed period of the drift as in **Figure 1b**.

increase in density, primarily set by salinity here, over a few meters, which we refer to as the base of the surface mixed layer. Below, salinity increases further, but more gradually, that is, over tens of meters, with temperatures at or close

to the freezing point. This layer is called the Arctic halocline (teal in **Figure 2c**, Schauer et al., 1997; Rudels, 2012). In temperature and salinity space (i.e., TS-diagrams), the halocline appears as an increase in salinity close to the

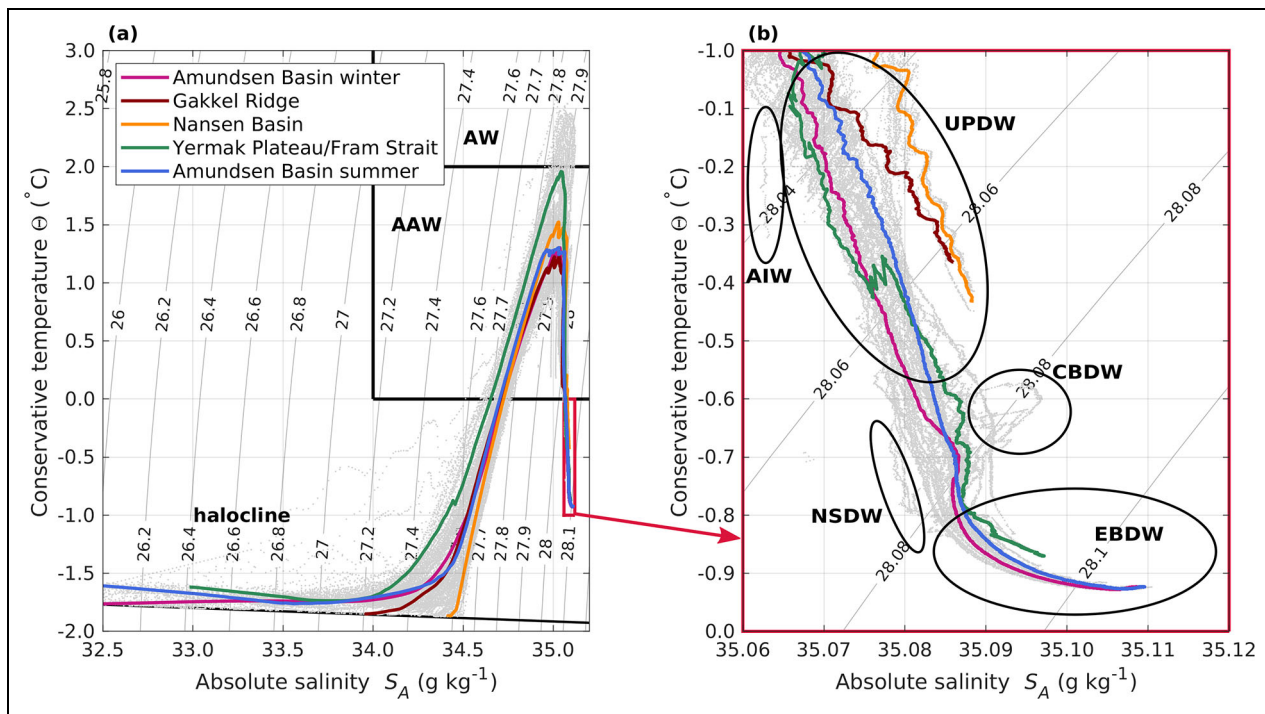


Figure 3. Temperature-salinity diagrams. Absolute salinity against conservative temperature for (a) the full depth range (for the basin averages, the upper 5 m are not shown) and (b) enlargement of the deep water masses. Gray lines indicate daily profiles and colored lines refer to basin averages as indicated. The black line in (a) indicates the salinity-dependent freezing point temperature, and black rectangles indicate Atlantic Water (AW) and Arctic Atlantic Water (AAW). The small pink rectangle in (a) corresponds to the range displayed in (b). In (b), circles indicate the approximate range of Upper Polar Deep Water (UPDW), Eurasian Basin Deep Water (EBDW), Canadian Basin Deep Water (CBDW), Arctic Intermediate Water (AIW), and Nordic Sea Deep Water (NSDW).

freezing point line (as in **Figure 3a**). Due to its strong stratification, the halocline suppresses the vertical exchange between the surface layer and underlying waters (Schulz et al., 2023a) and prevents both heat and nutrients from the Atlantic Water layer to reach the surface. In addition, the strong stratification also decouples the speed and even direction of lateral advection in the surface layer and halocline, which may all contribute to a heterogeneous distribution of tracers as well as microorganisms in these layers, despite both being located in the potentially sun-lit upper ocean.

Relatively warm and saline water from the Atlantic enters the Arctic Ocean through eastern Fram Strait and the shallow Barents Sea, carrying high nutrient concentrations (Torres-Valdés et al., 2013) and organisms of Atlantic origin (Snoeijs-Leijonmalm et al., 2022). This water circulates counterclockwise along the Arctic continental slopes (Schauer et al., 1997; Rudels, 2012) and is modified on its pathway by heat loss to the atmosphere when it resides close to the surface in the Barents Sea (Smedsrød et al., 2013; Meyer et al., 2017a) and subsequently by mixing with colder water masses (Lenn et al., 2009; Rippeth et al., 2015). This modification appears as a temperature decrease and a progressively deeper position of the warm and saline Atlantic Water within the water column along its advective pathway (e.g., Schulz et al., 2021). When Atlantic Water temperatures are below 2°C, we refer to it as modified, or Arctic Atlantic Water (AAW; beige in

Figure 2c). In TS-diagrams, this layer is visible as a temperature peak, that is, an increase and decrease of temperature over a narrow salinity range (**Figure 3a**). The distribution and modification of Atlantic Water can also be inferred from provenance tracers (e.g., Bauch et al., 2016; Laukert et al., 2017; Laukert et al., 2019).

The identification of deep waters below the Atlantic Water layer is less straightforward, as changes in temperature and salinity at these depths can be close to the instrument precision (as in the MOSAiC data, red box in **Figure 3**). Moreover, historical definitions for these deep waters might not hold anymore, as the properties of the water masses involved in their formation have been changing due to ongoing global warming (Somavilla et al., 2013; von Appen et al., 2015; Karam et al., 2024). Here, we use a set of historical definitions that differ between the central basins and the regions of Yermak Plateau and Fram Strait (see Section 2), but we advise treating these results with caution. In the central Eurasian Arctic Ocean (Amundsen and Nansen Basins), Upper Polar Deep Water (UPDW; lilac in **Figure 2c**) resides below the Atlantic Water layer. UPDW is a heterogeneous water mass formed as a mixture of intermediate waters, flowing into the Arctic Ocean through Fram Strait, and Atlantic Water that has been strongly cooled during winter in the Barents Sea, as well as saline and dense plumes formed on the shelves by brine rejection during sea ice formation (e.g., Rudels, 2009). In the TS-diagram, this water mass is

a mostly straight line with increasing salinity and decreasing temperature (**Figure 3b**). Below the UPDW, the primary water mass is Eurasian Basin Deep Water (EBDW; green in **Figure 2c**), with occasional intrusions of relatively warm and saline Canada Basin Deep Water (CBDW; pink in **Figure 2c**). EBDW is characterized by nearly constant temperature and is the result of the interaction between inflowing deep waters through Fram Strait and dense plumes from the shelves (e.g., Smethie et al., 1988). CBDW enters the Eurasian Basin across the Lomonosov Ridge and proceeds as a narrow boundary current but is episodically transported into the interior basin by eddies (Karam et al., 2023). The water mass close to the seafloor is called Eurasian Basin Bottom Water (EBBW; dark purple in **Figure 2c**); its properties are impacted notably by dense overflows and geothermal heating (e.g., Smethie et al., 1988). In Fram Strait, there is Arctic Intermediate Water (AIW; orange in **Figure 2c**) instead of UPDW below the Atlantic Water layer and Norwegian Sea Deep Water (NSDW; brown in **Figure 2c**) closer to the sea floor. AIW is characterized by nearly constant salinity and decreasing temperatures with depth and is typically enriched in oxygen, as it is formed through open ocean convection in the Nordic Seas (e.g., Meyer et al., 2017b). NSDW used to be seen as a cold, fresh, and very dense water mass but has warmed rapidly since the cessation of Nordic Seas deep convection, as it is no longer replenished. It now closely resembles EBDW (von Appen et al., 2015; Karam et al., 2023). All the deep water masses are different mixtures between water of Atlantic origin and waters entrained by deep convection (NSDW) or dense water overflows (all Eurasian basins deep waters) and therefore have different tracer properties, especially oxygen (Karam et al., 2023) and transient tracers (Heuzé et al., 2023a).

4.2. Surface and subsurface layer properties along the MOSAiC drift

The Amundsen Basin of early winter 2019–2020 was characterized by a well-defined surface mixed layer close to the freezing point down to around 30 m depth and a stable halocline below (**Figure 4a, d**). Intermediate surface salinities around 33 g kg^{-1} combined with low CDOM concentrations (**Figure 4b, c**) suggest that the contribution of river water was relatively small here. This small contribution could be related to different freshwater sources and their respective advective pathways, as the distribution of neodymium isotopes indicates alternating freshwater domains in this region reflecting variable contributions from the Yenisei, Ob, and Lena rivers (G Laukert, personal data). Sea ice meltwater from the preceding melt season may have also contributed to a fresher surface layer in this region (compared to the water below) and diluted the river-borne compounds. This dilution effect could explain the rather low dissolved organic carbon (DOC) concentrations at the very start of the drift (Kong, 2022). At the beginning of December, a decrease in salinity and an increase in both CDOM and river water fraction (derived from $\delta^{18}\text{O}$; see Section 2, Text S1) to over 13% indicate that the floe had

entered the river water-rich part of the Transpolar Drift. Somewhat surprisingly, the position of the maximum river water fraction does not coincide with the highest concentrations of CDOM, which appear only when surface salinity increases again and the surface layer started to deepen in March (**Figure 4a–c**). This disjunct could be related to different freshwater sources and their respective advective pathways, as the distribution of neodymium isotopes indicates alternating freshwater domains in this region either reflecting increased contributions from the Yenisei and Ob rivers or the Lena River (G Laukert, personal data). A similar but spatially shifted distribution has already been described based on summer data from 2015, suggesting a strong spatio-temporal variability of the surface waters in the Eurasian Arctic Ocean (Paffrath et al., 2021).

As it approached the Gakkel Ridge, the floe left the heavily river-water-influenced part of the Transpolar Drift and surface salinity increased to a maximum of 34.3 g kg^{-1} . River water fraction and CDOM concentrations decreased during the passage of the ridge (**Figure 4c**). These decreases were also coincident with a decrease of DOC concentrations in the surface layer (Kong, 2022). On the Nansen Basin side of the Gakkel Ridge, the surface mixed layer deepened to around 80 m. At the end of April, the surface stratification, that is, the halocline, disappeared completely and density only increased at a depth of approximately 130 m. These conditions have previously been described as “deep ventilation” (Polyakov et al., 2017), referring to a mixed layer that is not bounded by the halocline but reaches down to the warm Atlantic Water layer. This enhanced connectivity between the surface and Atlantic layer, compared to the situation in the Amundsen Basin, is also evident from provenance tracer distributions suggesting enhanced Atlantic Water admixture to the surface (G Laukert, personal data) and might promote the transport of deep oceanic heat toward the sea ice (see Section 6), thereby slowing basal growth (Lei et al., 2022), and increase vertical nutrient supply to the surface layer (Randelhoff et al., 2020). The enhanced vertical exchange might also facilitate the transport of organisms advected in the Atlantic Water layer closer to the surface. Deep ventilation, along with relatively constant surface salinity, low river water fraction, and CDOM concentrations, persisted throughout the Nansen Basin until the drift reached the Yermak Plateau in June (**Figure 4**).

Above Yermak Plateau, from the end of May onward, surface layer temperatures increased successively with ongoing solar warming and deviated more and more from the freezing point (**Figure 4b**). River water fraction and CDOM remained at the same low levels as encountered in the Nansen Basin, but a slightly lower surface salinity allowed for the presence of a halocline. The Atlantic Water layer on the eastern side and above the plateau was much shallower (see Section 4.3), restricting the vertical extent of the halocline (**Figure 4d**). Sea ice melt, starting in late May to early June (Lei et al., 2022; Webster et al., 2022), and surface warming created vertical density differences, that is, stratification, within the near-surface layer. Turbulent mixing in the upper ocean (see Section 6 for details) did not penetrate deeper than 30 m and usually was not

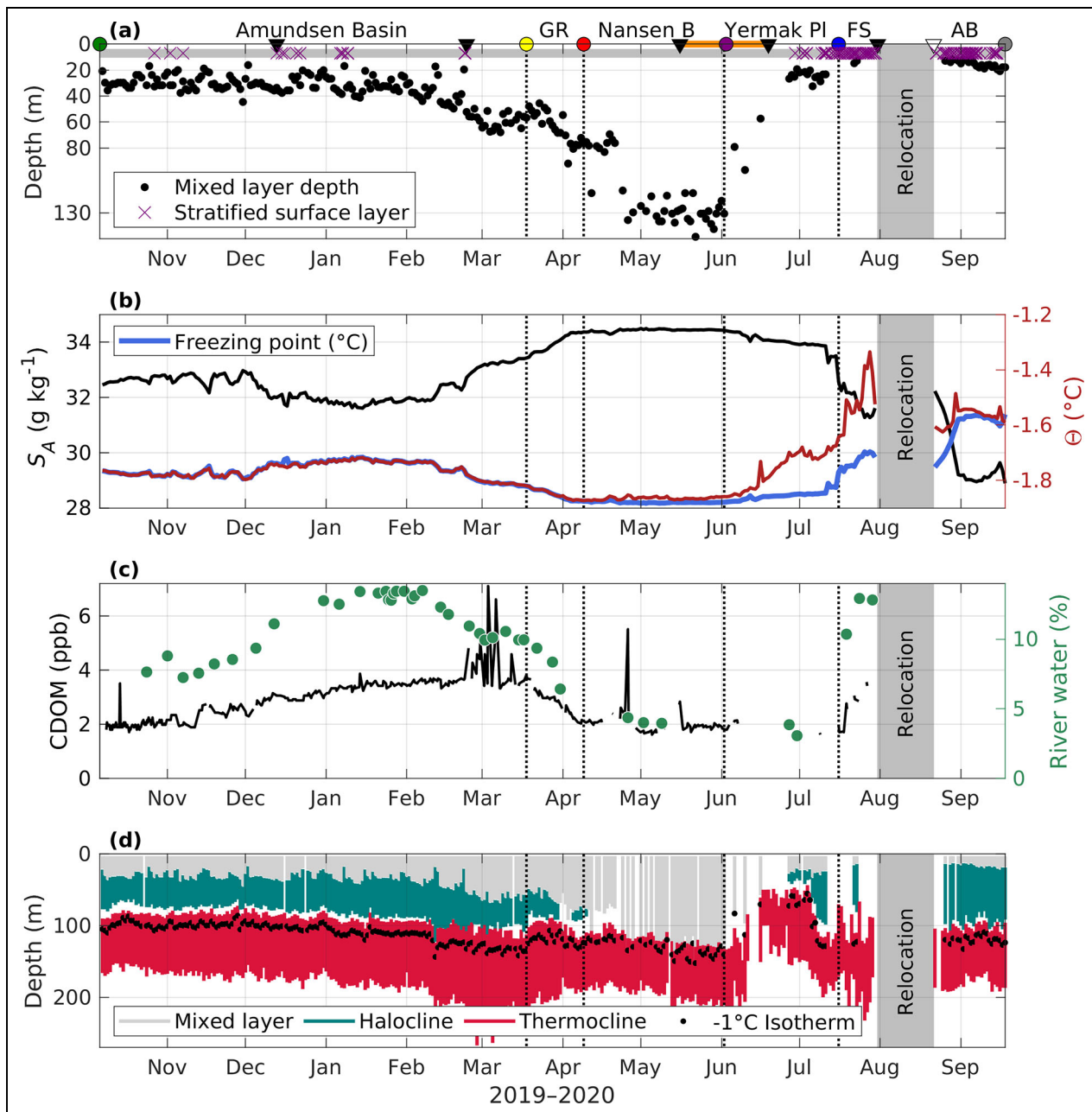


Figure 4. Ocean surface layer properties along the drift. (a) Surface mixed layer depth (m, black dots; stratified surface layers are indicated with purple crosses), (b) surface absolute salinity (g kg^{-1} , black line), conservative temperature Θ ($^{\circ}\text{C}$, red line), and freezing point temperature ($^{\circ}\text{C}$, blue line), (c) colored dissolved organic matter (CDOM; ppb, black line) and river water fraction (%), green dots), and (d) mixed layer (gray), halocline (teal), and thermocline (red) extent and position of the -1°C isotherm (black dots) along the drift. In (a), triangles indicate the start and end of the legs; dots, vertical dotted lines, and annotations, the geographical markers including Amundsen Basin (AB), Gakkel Ridge (GR), Nansen Basin (B), Yermak Plateau (PI), and Fram Strait (FS). The orange line indicates the uncrewed period of the drift as in **Figure 1b**.

strong enough to destroy the near-surface stratification established by meltwater input and warming. Hence, especially later in the season, we often observed no classical surface mixed layer (purple crosses in **Figure 4a**) and, even in the uppermost layer, vertical gradients in any tracer concentration, for example, nutrients, or organism distribution, can be expected.

When leaving the Yermak Plateau on July 16, we observed another regime shift in the surface layer:

Surface salinity abruptly decreased, while river water fraction and CDOM concentrations, which had remained low since entering the Nansen Basin, increased. This change is accompanied by a trend toward less radiogenic neodymium isotopic compositions (G Laukert, personal data), suggesting increased admixture of Lena River water and supporting cross-Arctic transport of Siberian freshwater. In Fram Strait, we also observed a subsurface increase of CDOM (data not shown), indicative of the

“edge” of the East Greenland Current (which is an extension of the Transpolar Drift of relatively fresh water of Siberian origin). Such a transition from one oceanic (surface) regime to another is often accompanied by sudden changes in biogeochemical water properties (e.g., nutrient relationships) and potentially also the ecological community structure (e.g., Tippenhauer et al., 2021). The surface temperature anomaly relative to freezing point further increased, to a maximum of 0.4°C shortly before the floe broke up.

After relocating north at the end of August, back into the Amundsen Basin, we observed the freshest surface waters (see also Rabe et al., 2022) and a stable halocline similar to the first phase of the drift. There are no sensor-based CDOM measurements after the relocation, but the highest CDOM absorption and DOC concentrations in surface waters during MOSAiC were found here (Kong, 2022). Moreover, the highest river water fractions based on oxygen isotopes and the least radiogenic neodymium isotope signatures were determined, in line with the strongest Lena River contributions during the entire MOSAiC campaign (G Laukert, personal data). The similarity of neodymium isotope signatures between this freshwater domain and that in the western Fram Strait may suggest continuous freshwater transport along the Transpolar Drift. However, enhanced freshwater export from the Siberian shelf exhibits a strong seasonality linked to the variable shelf hydrography (Janout et al., 2020), which may be preserved along the Transpolar Drift. The uppermost layer was often stratified due to sea ice melt and solar warming. Whenever a well-defined surface layer existed, it was about 20 m deep, slightly shallower than during the first part of the drift. Surface temperatures were still above freezing when sampling resumed, but approached freezing point at the beginning of September.

When sampling was resumed after the floe had been left uncrewed in July, we observed an approximately 1 m thick, low-salinity (S_A from close to 0 to about 10 g kg⁻¹) under-ice meltwater layer, visible in salinity profiles (Schulz et al., 2022b). At the interface between the fresher meltwater layer and the underlying colder seawater, thin layers of ice formed, so-called false bottoms (Smith et al., 2022; Salganik et al., 2023a). Low salinity meltwater layers in leads remained present until strong winds caused enhanced mixing during the period September 5–9 (Nomura et al., 2023; Smith et al., 2023). The presence of meltwater resulted in a very strong stratification in the uppermost meters, up to two orders of magnitude stronger compared to the halocline. Measurements with an uprising turbulence profiler also show drastically reduced turbulent mixing in the near-surface layer when meltwater layers were present (Fer et al., 2022). Details on the dynamics and implications of meltwater layers can be found in Smith et al. (2022), Nomura et al. (2023), Salganik et al. (2023a), and Smith et al. (2023).

4.3. Atlantic Water layer along the MOSAiC drift

Modified Arctic Atlantic Water (AAW) was present throughout the MOSAiC drift. In the Amundsen Basin, the upper limit of the AAW layer were situated at

approximately 150 m depth. After passing the Gakkel Ridge into the Nansen Basin, the AAW was warmer and situated deeper in the water column (**Figure 2a**). Relatively unmodified Atlantic Water (AW), coming straight from the Atlantic and being characterized by a core temperature above 2°C, was only present above Yermak Plateau (**Figure 2c**), where warm waters also resided about 100 m closer to the surface (**Figure 4d**), and in Fram Strait. Here, we use the term Atlantic Water (layer) to refer to both AW and AAW.

The “older” the Atlantic Water layer, that is, the longer it has been out of contact with the surface and traveled in the Arctic while being mixed with colder waters, the deeper and colder its core (Rudels, 2015). Hence, we observed a strong correlation ($R^2 = 0.67$, not shown) between the core depth and the core temperature. Along the drift in 2019–2020, the Atlantic Water core was mostly located at around 300 m depth, with a temperature around 1.2°C. Above Yermak Plateau and in Fram Strait, the core was approximately 1°C warmer (and 0.1 kg m⁻³ lighter) and 100 m shallower, but subject to strong variability. In this region, the impact of the shallow and “young” Atlantic Water on, for example, nutrient supply or organism composition might be more pronounced compared to the situation in the deep basins.

As Atlantic Water can take different paths within the Arctic Ocean, for example, entering via Fram Strait or through the Barents Sea, or recirculating into the deep basins from different positions along the continental slope (Rudels, 2012, 2015), different branches of Atlantic Water, with slightly different temperature and salinity signatures, can often be found at the same position, stacked on top of each other (Rudels and Hainbucher, 2020). These “interleaving” layers can be identified as z-shapes near the Atlantic Water temperature maximum in the TS-diagrams (**Figure 3a**) and as inversion layers and local temperature minima in the temperature profiles. In the Amundsen and Nansen Basin, interleaving involved mainly the Barents Sea and the Fram Strait branches of Atlantic Water. In the more dynamic Fram Strait region, we found strong interleaving, with several sources of Atlantic Water, which might differ in their respective biogeochemical signature that cause vertical gradients in, for example, nutrient concentration.

At the upper bound of the Atlantic Water layer, both temperature and salinity increase with depth. In quiescent conditions, that is, when turbulent mixing is negligible and molecular diffusion is the dominant mixing process, temperature gradients diffuse faster than gradients in salinity. This difference in thermal and haline diffusion coefficients creates step-like structures, so-called thermohaline or double-diffusive staircases, typical for the Arctic Ocean (Shibley et al., 2017). These structures can persist for years and over 100 km of horizontal distance, and individual layers can be up to several tens of meters thick (e.g., Lenn et al., 2009; Guthrie et al., 2017). Along the MOSAiC drift, we frequently, but not always, observed thermohaline staircases in the quiescent Amundsen Basin, in line with findings from high resolution observations from drifting stations in the same area, that show

1–3 m thick thermohaline staircase layers in the 200–260 m depth range (Sirevaag and Fer, 2012). Outside of the Amundsen Basin, we sometimes observed structures that might be remnants of thermohaline staircases in the vertical profiles (not shown), but their characteristic sharp interfaces were absent. These differences point toward a lower connectivity between the surface and deeper ocean in the Amundsen Basin, compared to the other parts of the drift.

4.4. Deep water along the MOSAiC drift

The deep water masses during the MOSAiC drift have been described in detail in Karam et al. (2023) and Rabe et al. (2022); here, we provide only a brief summary. Despite the uncertainties associated with the identification of deep water masses (sensor accuracy, changes in end member properties; see Section 4.1), we observed a somewhat consistent distribution of deep waters across the Eurasian basin during MOSAiC. In the Nansen and Amundsen Basin, UPDW was observed right under the Atlantic layer down to approximately 1500 m. Below the UPDW, primarily EBDW is found until the sill depth of Fram Strait (approximately 2500 m), with occasional intrusions of relatively warm and saline CBDW as a salinity maximum between 1700–2000 m depth (Karam et al., 2023). Below the sill depth of Fram Strait, the temperature increased slightly as we encountered the last deep water mass, EBBW, until the seafloor. Deep waters directly above the Gakkel Ridge and their unique hydrothermal-vent-influenced ecosystem were not sampled during MOSAiC.

The deeper waters above the Yermak Plateau and in Fram Strait consisted of UPDW, alternating with likely AIW. Below UPDW AIW, we again observed CBDW in Fram Strait, as a salinity maximum at roughly 2000 m depth. Close to the bottom in Fram Strait, we found a mixture of NSDW and EBDW. Again, we note that identifying water masses in Fram Strait solely based on their temperature and salinity signature as done in this study is associated with large uncertainties, primarily due to the warming and increased salinity of waters south of Fram Strait over the past decades. Hence, traditional water mass classifications (Marnela et al., 2016) do not necessarily hold for the deep waters anymore (Somavilla et al., 2013; von Appen et al., 2015). Other tracers, such as CFC, SF₆, or dissolved oxygen, are needed to accurately determine the origin of deep water masses, which is beyond our scope but addressed in Karam et al. (2023) and Heuzé et al. (2023a).

5. Current velocities, tides, and eddies

In both central basins, current velocities below the surface mixed layer were small, on the order of 0.01 m s⁻¹. Within the surface mixed layer, current velocities were intensified and correlated with the sea ice drift speed ($R^2 = 0.9$; data not shown). The magnitude of the ocean surface current (14–30 m vertical average), however, was much smaller, on average 16% of the floe drift speed (Figure 5a), meaning that the ice moves around six times faster than the upper ocean. This difference illustrates that, while both sea ice and fresh, riverine water are transported from their region of origin in Siberia across the Arctic toward Fram

Strait, their transport timescales and exact pathways differ. Sea ice within the Transpolar Drift typically traverses the Arctic Ocean within 1–3 years (Steele et al., 2004; Charette et al., 2020), while the transport timescale for freshwater might be rather on the order of a decade. In addition, the pathway of the Transpolar Drift is strongly influenced by daily to decadal variability in wind conditions (Mysak, 2001), yielding that liquid and solid freshwater of similar origin in space and time might take very different routes through the Arctic Ocean. The difference in sea ice drift and surface ocean current speed also underlines that, while sampling the same sea ice, the water below the ice quickly changes throughout the drift and oceanic data cannot be treated as a simple time series. Furthermore, as the surface mixed layer tends to move faster than the ocean below, any time series recorded above and below the surface mixed layer base might develop independently of each other.

The region around the Yermak Plateau and especially in Fram Strait is more energetic. Absolute current velocities were much higher (up to 0.4 m s⁻¹) and more variable, and surface currents correlated less with sea ice drift. Here, tides play a greater role, with a dominance of diurnal frequencies above the Yermak Plateau and semi-diurnal frequencies in Fram Strait (data not shown; see Fer et al., 2015, for details on tides in the region). In combination with the more variable water column structure in this region (see Section 4), we expect more variability on short, daily to sub-daily, timescales, for example, in surface nutrient supply or species composition. Assumptions of lateral homogeneity, that is, negligible spatial gradients, which are to some degree justified in the respective deep basins, no longer hold in the dynamic regime of the Yermak Plateau and Fram Strait.

Six upper ocean eddies were identified in the halocline in the Amundsen and Nansen Basin, listed in Table 2 and indicated in Figure 5b. Five of these eddies rotated anticyclonically (clockwise) and only one cyclonically, in line with the previously reported prevalence of anticyclonic eddies in the Arctic Ocean (Zhao et al., 2014; von Appen et al., 2022). The timing of these eddies does not coincide with the presence of storms or strong winds, indicating that the eddies had not been formed locally, but might rather be advected and originate from topographic features (Zhao et al., 2014) or barotropic and baroclinic instabilities (von Appen et al., 2022). Eddies can transport water masses with distinct biogeochemical signatures over large distances, and their associated higher current velocities can increase local vertical mixing (Son et al., 2022). Both processes can enhance the nutrient supply to the photic zone, making eddies potential biological hotspots. A presumably high fraction of nutrients supplied by eddy activity in the Arctic winter would not be consumed, but would instead (locally) increase the nutrient inventory for the next productive season. In addition, anticyclonic eddies are associated with a shoaling of the mixed layer base, which was most pronounced for the eddies in January and February when the mixed layer depth decreased by 10–20 m. However, a similar variability in mixed layer depth is also observed during times when eddies were

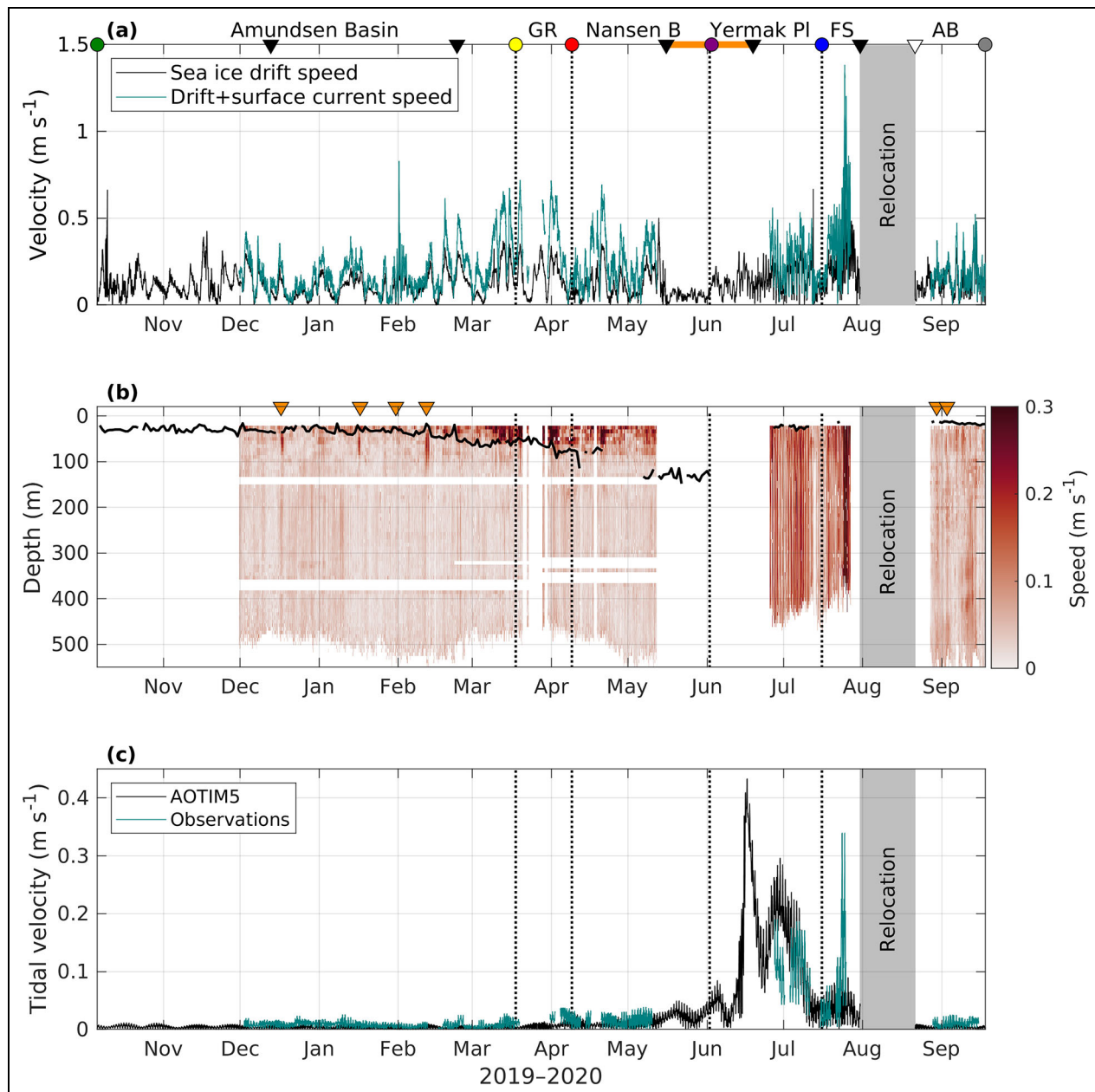


Figure 5. Current velocities along the drift. (a) Sea ice drift (black, m s^{-1}) and combined drift and averaged current velocity in the upper 14–30 m relative to the floe (teal, m s^{-1}), (b) current speed (m s^{-1}) relative to the sea floor, and (c) tidal velocities (m s^{-1}) from observations (teal) and the Arctic Ocean Tidal Inverse Model AOTIM5 (black) along the drift. In (a), triangles indicate the start and end of the legs; dots, vertical dotted lines, and annotations, the geographical markers including Amundsen Basin (AB), Gakkel Ridge (GR), Nansen Basin (B), Yermak Plateau (PI), and Fram Strait (FS). The orange line indicates the uncrewed period of the drift as in **Figure 1b**. In (b), orange triangles indicate near-surface eddies, the black line indicates the depth of the surface mixed layer.

absent. In the Yermak Plateau Fram Strait regions, eddy activity is obscured by the strong tides; hence no eddies were identified there.

On November 9, 14, and 28 (2019), we also observed a large anticyclonic eddy at greater depth in the middle of the Amundsen Basin, indicated by sloping isopycnals above and below the eddy, with relatively dense waters above the eddy and light waters below, relative to the adjacent water column (data not shown). This eddy carried a warm and saline CBDW intrusion and extended over approximately 1200–2400 m depth (Karam et al., 2023).

6. Turbulence and vertical transport

6.1. Surface mixing

In contrast to the surface *mixed* layer depth, which describes the depth to which the surface layer is uniform in temperature and salinity (see Section 4.2), the *mixing* layer depth describes how deep active turbulent mixing, which is created by friction at the ice-ocean interface, or by wind and waves in the marginal ice zone or open water conditions, penetrates into the water column. While active mixing creates the mixed layer by homogenizing the water column, the mixed layer will persist even after the

Table 2. Clearly identifiable upper ocean eddies along the drift

Start	End	D ^a (m)	Δh ^b (m)	Type
17.12.19 01:00	18.12.19 11:00	38	40	Anticyclonic
16.01.20 07:00	17.01.20 10:00	38	48	Anticyclonic
31.01.20 08:00	02.02.20 07:00	22	56	Anticyclonic
11.02.20 14:00	13.02.20 12:00	22	80	Anticyclonic
29.08.20 17:00	30.08.20 17:00	38	40	Cyclonic
03.09.20 23:00	03.09.20 10:00	30	64	Anticyclonic

^aFirst depth where the eddy was detected.

^bVertical eddy thickness.

active mixing has decayed. This persistence is because, even though the small-scale turbulent motion causing the mixing will dissipate within hours or days, the re-establishment of gradients near the surface, that is, restratification, often takes much longer, especially in the absence of restoring forces, such as strong lateral gradients. This delay explains why the distribution of biological and biogeochemical tracers is often homogeneous in the actively mixing layer, but not in the mixed layer, where it instead reflects a combined signal of past active mixing and new biological production (or consumption) in the respective layers (Caranza et al., 2018).

The relation between the depth of the mixed layer and depth of the active mixing layer is illustrated in **Figure 6a**. At times during MOSAiC, active mixing reached down to the base of the mixed layer, but was often confined to the upper 20 m. In the Nansen Basin, in the presence of deep ventilation conditions, active mixing occasionally reached to a maximum depth of 80 m, but not to the mixed layer base located at approximately 130 m. However, we have limited observations of turbulence here, due to the interruption of the drift between Legs 3 and 4. Upon return to the Amundsen Basin in summer, the mixed layer depth was shallower compared to the winter condition, caused by a lower surface salinity and hence stronger upper ocean stratification (teal line; **Figure 6a**). The active mixing layer depth, however, is comparable to the maximum depth of active mixing typically observed in this region in winter, during the first part of the drift, and reaches *deeper* than the mixed layer base. In other words, the same level of turbulent energy that created an approximately 30 m deep mixed layer in the presence of weaker upper ocean stratification (first part of the drift), only created a 20 m deep mixed layer in the presence of stronger stratification (last part of the drift). This comparison illustrates how strong stratification requires more turbulent energy to be mixed and that storm events, associated with elevated levels of turbulence, can have a different impact on the vertical transport of, for example, nutrients and other biogeochemical compounds or organisms, depending on the strength of the upper ocean stratification.

As the turbulent energy in the mixing layer mainly originates from friction at the ice-ocean interface, the depth of the mixing layer is, to a large extent, related to the sea ice

drift speed. A parameter to describe the impact of drift speed on upper ocean turbulence is the friction velocity, u_* (right vertical axis in **Figure 6b**). In the (winter) Amundsen Basin and in the Nansen Basin, the evolution of the mixing layer depth corresponds to variations in friction velocity, on a daily time scale. The relationship is different, but still visible, above the Yermak Plateau and breaks down in Fram Strait. Both regions were characterized by considerably higher current velocities, which likely contributed to the friction at the ice-ocean interface. Furthermore, sea ice melt probably reduced the bottom roughness of the sea ice (which was kept constant in the u_* calculation here), thereby reducing the efficiency of energy transfer from sea ice drift to surface ocean turbulence. After resuming sampling on another ice floe in the Amundsen Basin in late summer, in the presence of a stronger upper ocean stratification, the mixing layer depth was relatively constant and the effect of the friction velocity less clear. In summary, variations in ice drift speed strongly influenced the mixing layer depth on daily or probably shorter time scales, but other effects like the upper ocean stratification and tides are likely to alter this relationship.

The different timescales on which the active mixing depth and the mixed layer depth vary can have implications for the distribution of tracers and organisms in the near-surface layer. During longer calm periods, when the wind and drift speed are low, vertical biogeochemical gradients might be established within the surface mixed layer, for example, if nutrients are preferentially consumed in the upper part of the mixed layer, where more sunlight is available, or if tracers and organisms from melting sea ice are injected to the ocean and accumulate only in the very top layer. A wind event could then easily homogenize these gradients on very short (hourly) timescales, altering the biogeochemical signature over the whole mixed layer depth. Such an event could boost primary productivity, by replenishing surface nutrients, but could also have an adverse effect by displacing organisms to greater depths, where less sunlight is available and food is more diluted.

6.2. Turbulent diffusivity

The decay of turbulent energy with increasing distance from the surface, where it is generated mainly by friction under the sea ice, is visible in **Figure 7a**. In the Amundsen

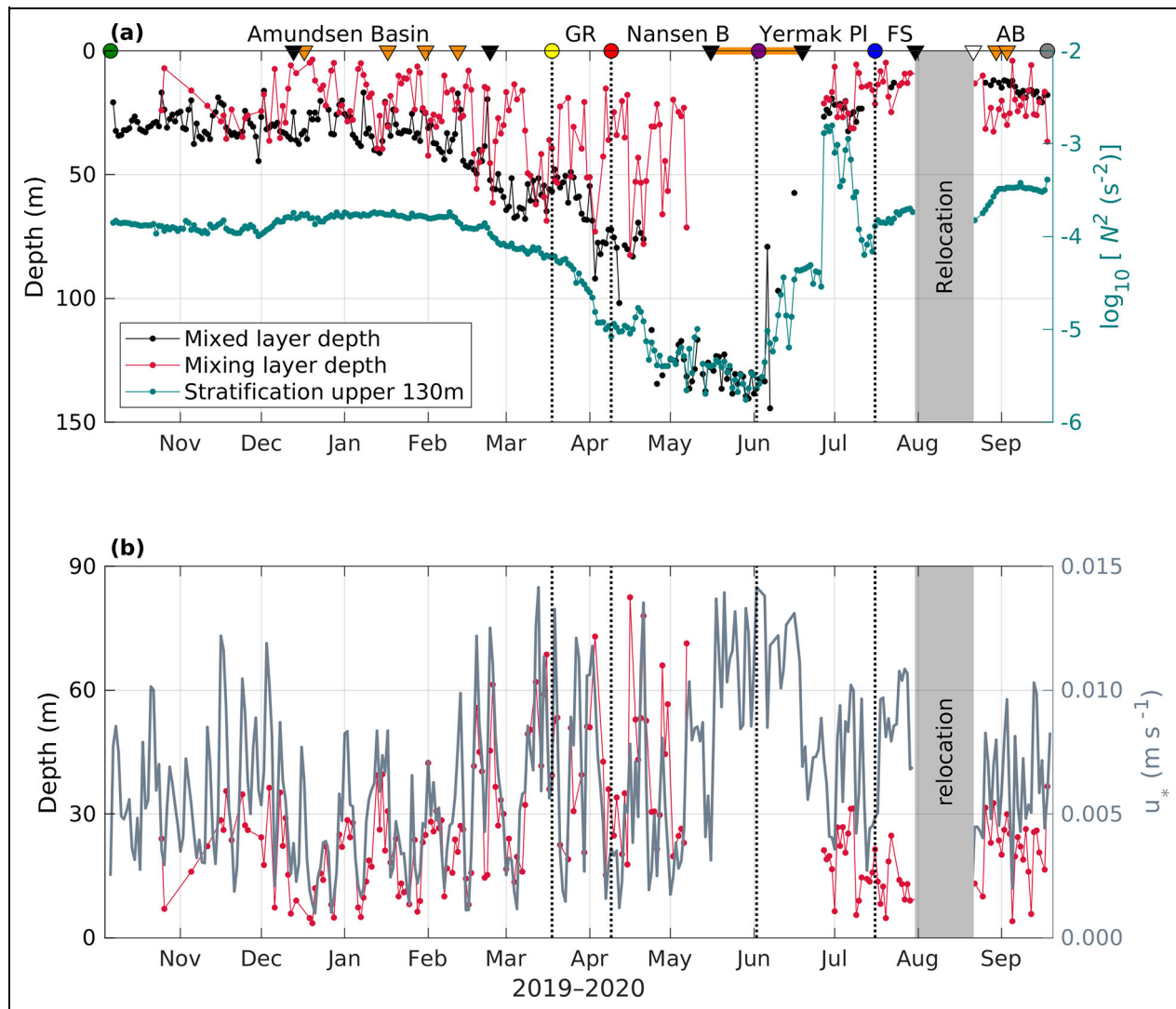


Figure 6. Parameters related to surface turbulence along the drift. (a) Surface mixed layer depth (black) and mixing layer depth (red, m, left vertical axis) and upper ocean stratification (teal, right axis, s^{-2}). (b) Mixing layer depth (red, m, left axis; note that the vertical axis is reversed) and friction velocity (gray, right axis). In (a), black and white triangles indicate the start and end of the legs; dots, vertical dotted lines, and annotations, the geographical markers including Amundsen Basin (AB), Gakkel Ridge (GR), Nansen Basin (B), Yermak Plateau (PI), and Fram Strait (FS). The orange line indicates the uncrewed period of the drift as in **Figure 1b** and orange triangles indicate near surface eddies.

Basin, strong stratification (**Figure 7b**) confined elevated levels of mixing to the upper approximately 70 m in winter and, due to stronger surface stratification, to approximately 50 m in summer. In the Nansen Basin, where the upper ocean was well mixed or only weakly stratified (yellow lines in **Figure 7**), turbulence was elevated in the upper 90 m and still slightly above noise level down to approximately 200 m. The Yermak Plateau and Fram Strait regions were more stratified, partly due to buoyancy input by meltwater and solar warming, but also more dynamic (see Section 5). Here, turbulence was strongly elevated in the upper 40 m and still elevated below, though weaker than in the Nansen Basin.

Vertical diffusivity, the coefficient necessary to calculate turbulent vertical fluxes in the presence of stratification, differed both regionally and depending on the vertical position in the water column. In the strongly

stratified halocline in the Amundsen Basin, values are smallest and on the order of $10^{-6} m^2 s^{-1}$, as already reported in Schulz et al. (2023a), illustrating how the halocline separates the surface from the deeper water layers. In the conditions we encountered in summer, characterized by lower surface salinity and a shallower mixed layer, the “bottleneck” for vertical transport formed by the halocline was even more pronounced (blue and violet lines in **Figure 7c**). In the Yermak Plateau and Fram Strait regions, upper ocean (30–160 m) vertical diffusivity was an order of magnitude higher, around $10^{-5} m^2 s^{-1}$ (green line in **Figure 7c**). In the Nansen Basin, upper ocean vertical diffusivity is highest, ranging from more than $10^{-3} m^2 s^{-1}$ in the upper 50 m and gradually decreasing to approximately $10^{-5} m^2 s^{-1}$ at around 170 m depth. Highest vertical fluxes of any tracer, for example, heat, nutrients, or oxygen, can therefore be expected in the Nansen Basin.

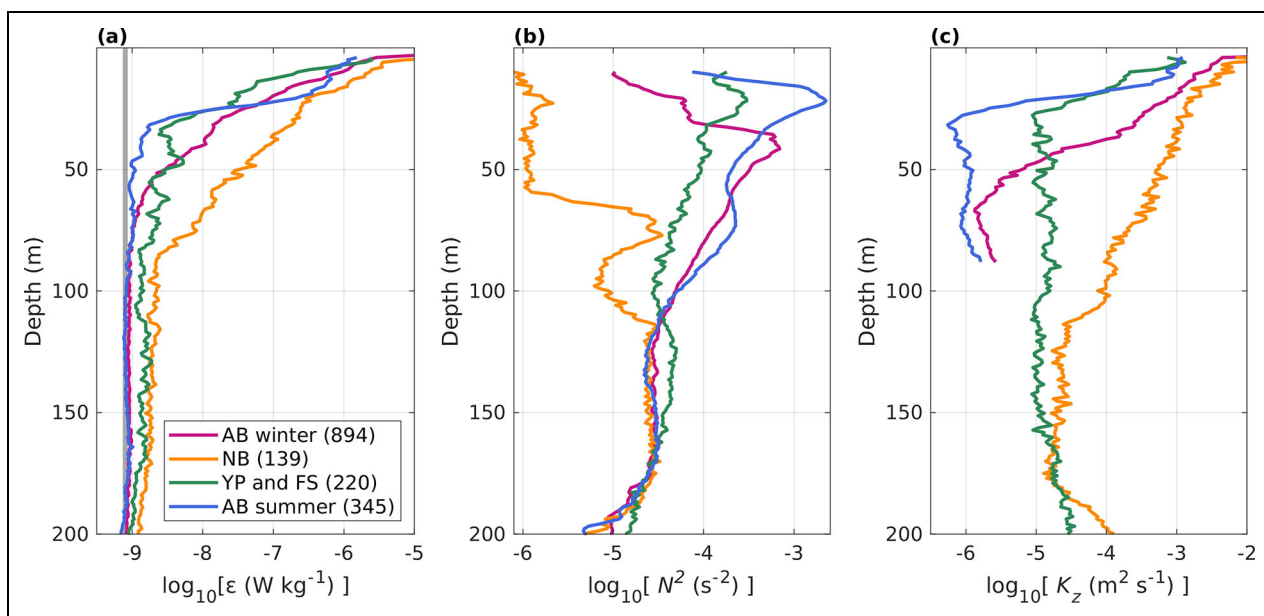


Figure 7. Turbulence and stratification profiles. Basin-averaged vertical profiles of the (a) turbulent dissipation rate ϵ (W kg^{-1}), (b) Brunt-Väisälä frequency, N , squared (s^{-2}), and (c) vertical diffusivity K_z ($\text{m}^2 \text{s}^{-1}$). Colors refer to the Amundsen Basin (AB) summer and winter conditions, Nansen Basin (NB) and the Yermak Plateau (YP) and Fram Strait (FS) averages, the vertical gray line in (a) indicates the lowest detection (“noise”) level of the profiler. Data below around 90 m in the Amundsen Basin and below 200 m in the Nansen Basin and the Yermak Plateau and Fram Strait regions are at noise level and not shown in (c).

The variability within both basins was relatively low, with average values providing a good representation of the typical conditions. However, the Yermak Plateau and Fram Strait regions are energetic and exhibited considerably different conditions, for example, with respect to tidal currents (Section 5), stratification and Atlantic Water layer properties (Section 4). Here, average values can be informative and descriptive, but for detailed studies in those regions, the actual contemporaneous conditions need to be considered.

6.3. Heat fluxes

Ocean heat fluxes presented here were calculated in two ways. Close to the surface (3 m depth), high-resolution point measurements of three-dimensional velocity and temperature from an autonomous buoy provided heat fluxes based on direct eddy correlation methods. In deeper layers, we derived heat fluxes from vertical temperature gradients and the vertical diffusion coefficient K_z (described above), for example, over the halocline or the Atlantic Water thermocline (see Section 2, Text S1). The heat flux at 3 m reflects how a small difference in heat, that is, water even slightly above the local salinity-controlled freezing point, is transported near the ice-ocean interface. The heat flux over the halocline describes the heat entering the surface mixed layer from the ocean below. The heat flux over the thermocline can be interpreted as the heat lost from the Atlantic Water to the colder water layer above (Schulz et al., 2021). Similarly, vertical fluxes of other tracers, for example, nutrients or dissolved oxygen, could be calculated from the K_z data presented here and the respective tracer profiles.

Depending on the position of the layer of interest, for example, the nitrcline, we expect that these fluxes qualitatively follow the variability we observed in heat fluxes.

Heat fluxes at 3 m depth, near the top of the ocean mixed layer (Figure 8a), ranged between -2 W m^{-2} and 7 W m^{-2} , exhibiting a typical wide day-to-day variability, arising primarily from the variable wind-forced motion of the ice (Figure 5a). During the winter period, in the absence of solar heating, the 3 m fluxes arose from wind-ice-forced turbulent mixing of heat within the mixed layer and heat trapped by the strong salinity-controlled density gradient at the base of the mixed layer. Heat transport from the base of the mixed layer was strongly amplified in the presence of eddies. During the ice growth period (December to end of April), ice basal growth of 0.92 m to 1.05 m was measured (AOFB altimeter on a different floe; Perovich et al., 2023). This basal growth is dominated by ice conductive fluxes controlled by air temperature, humidity, wind speed, the effects of highly insulating snow, ice thickness, and ice salinity. Because the ocean mixed layer temperature is very close to the freezing point (Figure 4b; Section 4.2), heat lost to the ice cannot further cool the ocean, but rather forms ice, releasing brine and removing latent heat from the ice-water interface (e.g., McPhee, 2008). The small contribution to ice basal change from time-integrated predominantly upward heat fluxes for this time series was just 1.2 cm of ice loss, with little contribution after the beginning of May 2020.

As previously reported, based on the winter Amundsen Basin data from MOSAiC (Schulz et al., 2023a), the heat flux over the halocline is negligible, meaning that the

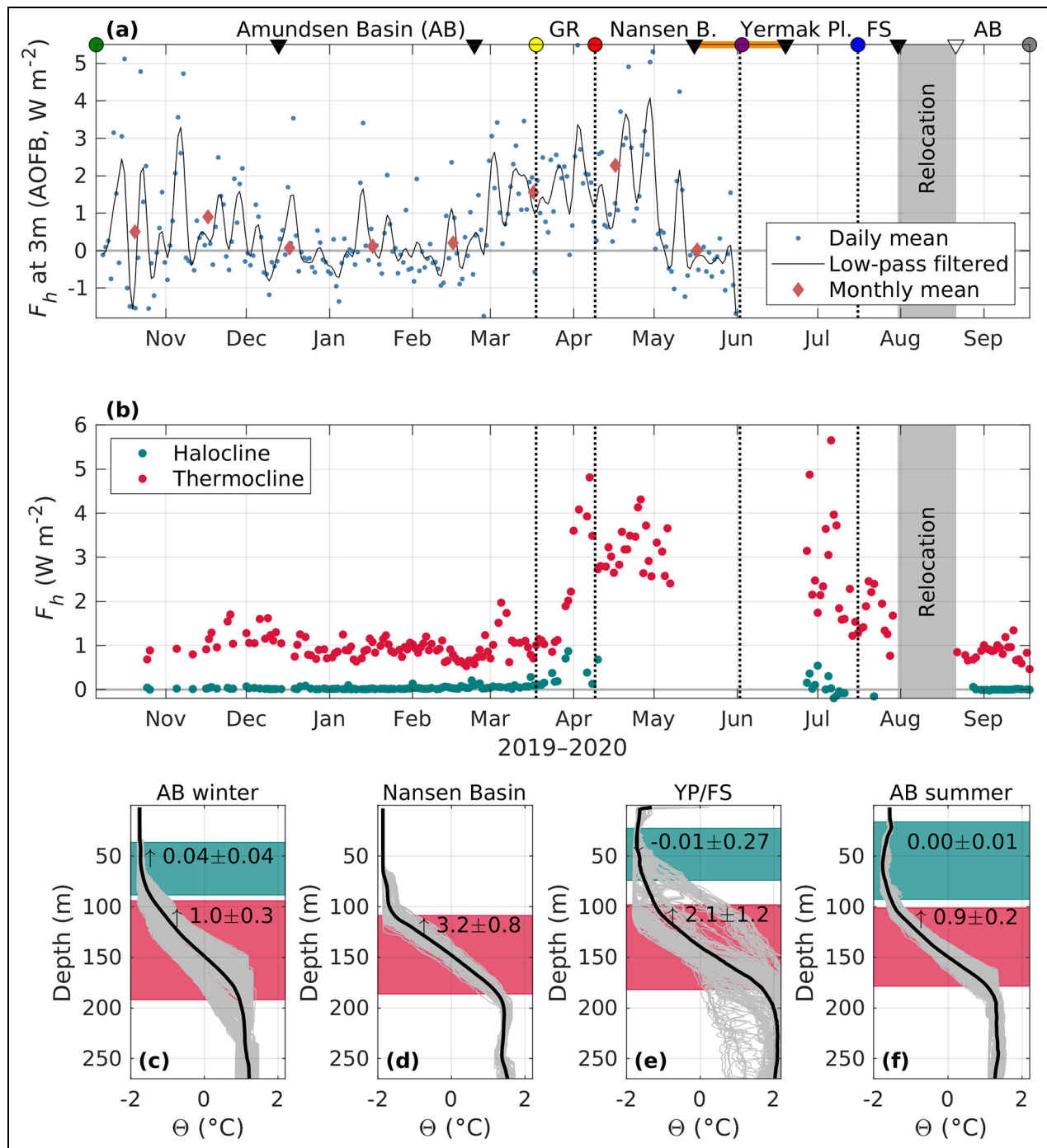


Figure 8. Vertical heat fluxes during the drift. (a) Heat fluxes (F_h) at 3 m depth, based on eddy-correlation, measured with an Autonomous Ocean Flux Buoy at the Distributed Network “L2” site (Rabe et al., 2022), at a distance of 15–25 km from *Polarstern*. Blue dots are daily averages; the black line is a 6-day low-pass filtered time series and red diamonds are monthly mean flux values. (b) Heat fluxes over the halocline (teal dots) and Atlantic Water thermocline (red dots) based on shear probe measurements. (c–f) Individual (gray) and average (black) conservative temperature (Θ) profiles and average halocline and thermocline heat fluxes in the Amundsen Basin (AB) in summer and winter, the Nansen Basin and the Yermak Plateau and Fram Strait regions (YP/FS). All values are in W m^{-2} . In (a), triangles indicate the start and end of the legs; dots, vertical dotted lines, and annotations, the geographical markers including the Gakkel Ridge (GR), Nansen Basin (B), Yermak Plateau (Pl), and Fram Strait (FS). The orange line indicates the uncrewed period of the drift as in Figure 1b.

halocline effectively shelters the upper water layers and the sea ice from the heat in the Atlantic Water layer. While there was a minimal upward flux in the Amundsen Basin

in winter, with heat fluxes much smaller than 0.1 W m^{-2} , the stronger stratification present in summer completely suppressed any heat transport over the halocline

(Figure 8a, c, f). As the Gakkel Ridge was approached in March, halocline heat fluxes gradually increased, reaching maximum levels above the ridge. However, daily mean values were still small, below 0.8 W m^{-2} (directed upward). Halocline heat fluxes above the Yermak Plateau were comparable to those above the Gakkel Ridge, until surface heating reversed the temperature gradient and small, downward-oriented heat fluxes were observed.

Upward heat loss from the Atlantic Water layer in the Amundsen Basin was around 1 W m^{-2} , with little (sub)-seasonal variability. Under deep ventilation conditions in the Nansen Basin, in the absence of a sheltering halocline, the more turbulent surface layer directly connects with the Atlantic Water layer and thermocline heat fluxes increased by a factor of three, compared to the Amundsen Basin conditions with a stable halocline (**Figure 8b, c, d, f**). In the Yermak Plateau and Fram Strait regions, heat fluxes were also enhanced, but the temperature structure in the water column, and hence the heat flux, was more variable (**Figure 8c**). Here, heat fluxes were highest on the plateau, where the Atlantic Water layer is shallow and the Atlantic Water core is warmer (and younger) compared to the rest of the drift. Heat fluxes decreased to a level between Nansen and Amundsen Basin conditions as Fram Strait was entered.

7. Comparison of MOSAiC data and ocean climatologies

Ocean climatologies are interpolations of observed temperature and salinity profiles, which are often used as initial or boundary conditions in modeling studies, or for ground-truthing the results of simulations. In contrast, state estimates are realizations of numerical models that have been optimized to best fit observational data, while obeying the physical laws that govern processes in the ocean. The majority of data used to create the climatologies were collected more than 10 years ago (**Table 1**). Because the Arctic is the world's fastest-changing region, it is unclear how representative these datasets still are. The high-resolution MOSAiC data can serve as a benchmark for the "modern-day" Eurasian Arctic, enabling an evaluation of how representative the climatologies are of the current conditions. Here, we compare four climatologies and two state estimates in three time periods regions (**Figure 9**) to the new MOSAiC data. We calculated month-long averages of the MOSAiC data, with the January average representing Amundsen Basin winter conditions, May representing spring conditions in the Nansen Basin, and July representing summer conditions in the Fram Strait region. The corresponding climatological averages were derived from the objectively analyzed monthly datasets of each climatology state estimate, utilizing the nearest climatology grid cell to the drift location at the midpoint of the corresponding month. For additional information, including details about the respective data sources for the climatologies, see Text S1.

Overall, we found good agreement between the climatologies and MOSAiC data, regarding the vertical structure and seasonal and regional variability. The MIMOC and WOA18 climatology show strong agreement

and similarity, despite WOA18 containing a larger proportion of older data compared to MIMOC. The two state estimates, ECCO and ASTE, accurately reconstruct the complex vertical structure and the halocline, as well as seasonal and regional changes. Not all climatologies accurately represent the surface mixed layer, which is subject to considerable short-term variability, as profiles were often averaged over different regions and time periods. MIMOC is the only climatology that considers this issue during the interpolation and objective mapping process.

PHC3, with the oldest data of all the data products considered here (**Table 1**), features a fresher Atlantic layer and halocline, compared to other data products and MOSAiC data, which is expected as most data are pre-Atlantification (Polyakov et al., 2017). The state estimates ECCO and ASTE are subject to temperature biases in the Atlantic layer, with ECCO being $1\text{--}1.5^\circ\text{C}$ colder and ASTE being $0.2\text{--}2.0^\circ\text{C}$ warmer (with a larger bias in spring summer Eurasian Basin than in the winter Amundsen Basin), compared to the observed Atlantic Water core. ASTE also exhibits a salinity bias, with a fresher Atlantic Water and halocline layer, resulting in a weaker stratification. These biases point to issues reproducing the Atlantic Water pathway (a common issue in many models, for example, Wang et al., 2023; Heuzé et al., 2023b), an underestimation of vertical heat fluxes from the Atlantic Water layer and not enough observations along the Eastern Arctic boundary current available to constrain the model (Nguyen et al., 2021). Constraining a new release of ASTE with MOSAiC data will likely reduce this bias.

Across all basins and seasons, the MOSAiC data consistently exhibit warmer Atlantic Water, compared to the climatologies. The climatologies demonstrate a clear temporal dependency, with PH3, containing the oldest data, featuring the coldest Atlantic Water, approximately 1°C colder compared to the most recent WOA23. This observation aligns with the expected consequences of rapid Arctic Amplification and Arctic Ocean warming (Rantanen et al., 2022). Another possible shift is indicated in the Amundsen Basin halocline properties, the extent of which decreases from 130–200 m in the (oldest) PHC3 climatology to 70–100 m during MOSAiC. This shift is in line with previous findings of a weakening and shallowing of the halocline over recent decades (Polyakov et al., 2020a).

However, MOSAiC data comprise a snapshot of only one year and do not capture interannual or decadal variability (e.g., Polyakov et al., 2023). The identification of long-term variability and or climate-change-induced changes in water mass properties at all depths is not trivial. It requires in-depth analyses of variability and changes in both the upstream (e.g., properties in and exchanges with the Nordic Seas) and the internal (e.g., shelf ventilation) processes. Such analyses can only be undertaken by comparing MOSAiC to several decades of scarce, historical data and are beyond the scope of this study. We also note that, consistent with previous studies (e.g., Timmermans and Marshall, 2020), we observed significant regional disparities within the Arctic Ocean, surpassing temporal variations on both short and long-term timescales. Therefore, while the MOSAiC data reflect conditions in the Eurasian

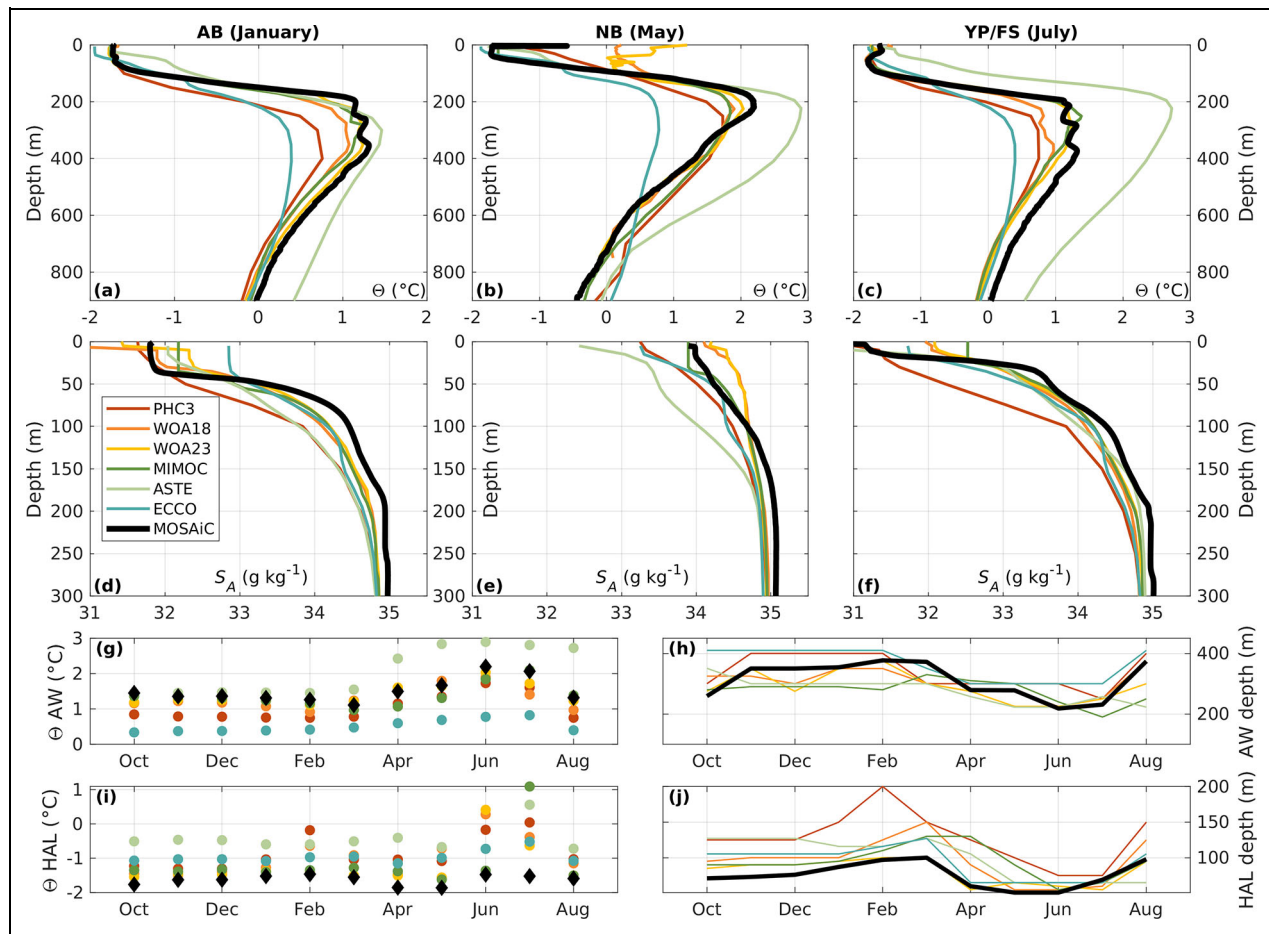


Figure 9. Comparison of the observations along the drift with climatological datasets and state estimates.

(a–c) Conservative temperature (Θ) and (d–f) absolute salinity profiles of four climatological datasets (PHC3, WOA18, WOA23, and MIMOC) and two state estimates (ECCO and ASTE; see Section 2 and Text S1 for definitions and details) and the MOSAiC observations. Note the different ranges on the y-axis for salinity and temperature. Data have been averaged for the months of January in the Amundsen Basin (AB), May in the Nansen Basin (NB) and July in the Yermak Plateau, and Fram Strait regions (YP NB). (g) Atlantic Water (AW) core conservative temperature (Θ) and (h) depth (m), and (i) halocline (HAL) conservative temperature (Θ), and (j) depth (m).

basins, they do not necessarily represent modern-day conditions elsewhere in the Arctic (see also Section 9).

8. Discussion

8.1. MOSAiC findings in comparison with previous results

8.1.1. Surface waters

Upper ocean properties along the MOSAiC drift were strongly influenced by the relative position of the sampling within or outside of the river water-rich Transpolar Drift. A direct comparison to earlier observations is challenging, as the exact pathway of river water is subject to seasonal and interannual variability (e.g., Mysak, 2001; Karcher et al., 2012) and sampling locations of previous expeditions or ITP drift tracks differ from the MOSAiC locations. At the beginning of the MOSAiC drift, the mixed layer salinity in the eastern Amundsen Basin, around 32 g kg^{-1} (Figure 4b), appears to be higher than in the early 2010s in the same area: Observations from late summer in 2011 (Polarstern expedition PS78; Gonçalves-Araujo et al., 2018) and 2012 (ITP64; Stedmon et al., 2021a) show

a fresher surface layer with salinity around 30 g kg^{-1} and a higher CDOM loading, indicative of larger presence of river runoff in the easternmost Amundsen basin. Similar conditions were observed in 2015 (Polarstern expedition PS94; Stedmon et al., 2021b). This difference in surface salinity and CDOM concentration might indicate that the first part of the MOSAiC drift was rather intersecting the “edge” of the river water-rich Transpolar Drift and not the core, where surface salinity would likely be closer to 30 g kg^{-1} , at least in late summer, and river water fraction would be closer to 20% (e.g., Bauch et al., 2011; Charette et al., 2020; Paffrath et al., 2021). The conditions observed after re-location closer to the North Pole (where the freshwater-rich part of the Transpolar Drift is often located), with surface salinities around 29 g kg^{-1} (Figure 4b), are more typical for the freshwater-rich part of the Transpolar Drift (e.g., Bauch et al., 2011; Charette et al., 2020). Provenance tracer data show that the river water component of the freshwater-rich part has a considerable proportion of Lena River water, while the lower river water fractions at the “edges” are mainly attributable

to contributions from the Yenisei and Ob rivers (G Laukert, personal data). These attributions are consistent with a shorter advection time of Lena River water into the central Arctic Ocean, resulting in less mixing with ambient water, and suggests significant differences in biogeochemical water properties even within the river water-influenced part of the Transpolar Drift.

8.1.2. Surface mixed layer depth

Peralta-Ferriz and Woodgate (2015) reported estimates of the mixed layer depth for the whole Eurasian Basin, using 519 profiles in the time period 1979–2012. Based on monthly averages, they found a maximum mixed layer depth of 73 m in April, but also observed depths of >100 m in winter and a minimum depth of 22 m in July–August. These ranges are similar to the conditions encountered during MOSAiC, given the high internal variability of the mixed layer depth. Peralta-Ferriz and Woodgate (2015) also highlighted that the Arctic mixed layer depth distribution is patchy and found a dominance of upper ocean stratification, rather than wind or drift speed, in determining the local mixed layer depth in ice-covered situations. Throughout the MOSAiC drift, we also found the mixed layer depth to be influenced strongly by the surface salinity, which to first order sets the upper ocean stratification. In the presence of a surface salinity below 30 g kg^{-1} , the maximum mixed layer depth was just over 20 m (Amundsen Basin, summer), whereas at a higher surface salinity of around 32 g kg^{-1} the surface mixed layer was as deep as 50 m. Deep ventilation, with a mixed layer depth of around 130 m, was observed only at a surface salinity greater than 34.1 g kg^{-1} (Nansen Basin). Winter deep ventilation has been observed previously (Polyakov et al., 2017) and was attributed to changes associated with Atlantification, for example, weakened upper ocean stratification, higher turbulence and enhanced heat fluxes. MOSAiC data show that these conditions were present everywhere along the drift track in the Nansen Basin. However, a similar disappearance of the halocline, related to a high surface salinity, was already observed in the eastern Arctic Ocean in the 1990s (Steele and Boyd, 1998) and found to be transient (Boyd et al., 2002).

8.1.3. Halocline thickness and stratification

Based on 18,000 profiles of ocean temperature and salinity collected during the period 1997–2008, Bourgoin and Gascard (2011) assessed properties of the Arctic halocline. Similar to the variability encountered during MOSAiC, they found the strongest, that is, most stratified, halocline layers close to the freshwater sources at the Siberian shelves. The weakest haloclines (together with the deepest mixed layers, down to 70 m) were found in the western Nansen Basin, where we encountered a deeper mixed layer and a complete absence of the halocline during MOSAiC. Bourgoin and Gascard (2011) found the halocline in the Amundsen Basin to be very stable during their investigated time period, with no clear seasonal variability, but their data coverage in winter was sparse. During MOSAiC, we found an apparent seasonal signal, with a thicker ($76 \pm 9 \text{ m}$ versus $50 \pm 11 \text{ m}$) and more stratified

($50 \pm 7 \times 10^{-5} \text{ s}^{-2}$ versus $28 \pm 8 \times 10^{-5} \text{ s}^{-2}$) halocline in summer, compared to the winter situation, which is attributed to a lower surface salinity in summer. However, while seasonal meltwater in the surface layer has an effect on the surface salinity, MOSAiC data indicate that the local surface salinity is set by the relative position within or outside the river-water influenced Transpolar Drift rather than by seasonality (see Section 4). Taking into account both seasons, the Amundsen Basin halocline got thinner ($55 \pm 14 \text{ m}$ versus $70 \pm 10 \text{ m}$) but more stratified ($32 \pm 12 \times 10^{-5} \text{ s}^{-2}$ versus $20 \pm 3 \times 10^{-5} \text{ s}^{-2}$) compared to the values reported in Bourgoin and Gascard (2011). Given the strong spatial gradients in surface salinity in the Amundsen Basin and the still limited spatial coverage of data, these differences could reflect internal variability rather than trends.

8.1.4. Heat fluxes

Heat fluxes near the ice-ocean interface (at a depth of 3 m) exhibited low values during the MOSAiC winter and displayed significant day-to-day fluctuations. This pattern aligns with the findings of Meyer et al. (2017a) in the Nansen Basin during the N-ICE2015 winter (at 1 m depth). Moving into early spring, specifically in May, the heat fluxes recorded by the AOFB buoy reached levels of around 5 W m^{-2} , a value that is consistent with the approximately 10 W m^{-2} reported by Meyer et al. (2017a) for the same month. In June, during the N-ICE2015 campaign, the fluxes ranged over $10\text{--}50 \text{ W m}^{-2}$, reaching peaks exceeding 300 W m^{-2} during storms that caused upward mixing of warm subsurface waters. Unfortunately, the MOSAiC data lack shallow measurements from June onward.

Heat fluxes across the halocline during MOSAiC were virtually zero, which is in line with previous findings (Fer, 2009), including from the SHEBA campaign in the Western Arctic (Shaw and Stanton, 2014). Also, the relatively low heat fluxes over the Atlantic Water thermocline found in Amundsen Basin match previously reported values in that region (Lenn et al., 2009; Schulz et al., 2021). The higher heat fluxes over the thermocline found in the Nansen Basin correspond to values of around 3 W m^{-2} found during N-ICE2015 (Meyer et al., 2017a) and elevated heat fluxes in the absence of a halocline, as observed in the Nansen Basin, have been reported previously (Steele and Boyd, 1998). Heat fluxes over the thermocline for June and July were generally confined to the range of $2\text{--}5 \text{ W m}^{-2}$, much lower than during N-ICE2015. This limited range is attributed primarily to the shallower warm Atlantic layer in the N-ICE2015 area compared to the MOSAiC location and the absence of storms during this period of the MOSAiC drift.

8.2. Interdisciplinary implications

The regional differences in physical hydrography encountered during the MOSAiC drift have various implications for other Arctic subsystems. In the following, we discuss how the variability in physical properties along the MOSAiC drift might shape the distribution of nutrients and the carbonate system, bio-optical properties, the

ecological structure across multiple trophic levels and sea ice and atmospheric processes.

8.2.1. Nutrient and carbonate system dynamics

Water masses, transport and turbulent mixing impact the distribution of nutrients, carbon, and other geochemical tracers. Nutrient inventories in the surface waters differ regionally, with signals being potentially larger than the seasonal signals of biological uptake and remineralization (Juranek, 2022), particularly in basins with longer ice-cover duration where the residence time of tracers is increased due to accumulation in surface waters (Eveleth et al., 2014). Similarly, for various carbonate system components, such as dissolved inorganic carbon (DIC) and total alkalinity (TA), a strong positive correlation is usually found with salinity (Friis et al., 2003), indicating that the marine carbonate system is closely related to physical water mass properties.

Atlantic Water, residing at depths greater than 100 m, forms the largest source of nutrients in the central Arctic Ocean and is an enormous reservoir of dissolved inorganic carbon (DIC), as organic matter from the sun-lit surface ocean eventually sinks and remineralizes. The transport of these nutrients and carbon up to the photic zone, where they can be utilized by primary producers, is strongly limited by the presence of the halocline, which acts as a barrier layer (e.g., Fer, 2009; Schulz et al., 2022a). When the halocline is absent and the mixed layer penetrates the Atlantic Water layer (Polyakov et al., 2017), ventilation can potentially create locally larger nutrient inventories at the start of the productive season and enhance the biological carbon drawdown (Juranek, 2022). These physical conditions were observed in the Nansen Basin (Section 4.2). Enhanced vertical nutrient transport might also occur when Atlantic Water resides high up in the water column (as on the Yermak Plateau; Section 4.3). On the other hand, vertical mixing of deep DIC during ventilation or passing eddies can partially offset biological CO₂ drawdown by increasing the partial pressure of CO₂ (pCO₂) in the surface layer (Bates and Mathis, 2009; Lannuzel et al., 2020).

Among marine carbonate system components, the surface layer pCO₂ is often the point of focus in sea-air CO₂ exchange studies, as it determines whether the ocean is a sink or source of CO₂ to the atmosphere. The Arctic Ocean is generally considered to be a CO₂ sink, as surface layer pCO₂ is often undersaturated relative to the atmosphere (Tanhua et al., 2009; Schuster et al., 2013; Fransson et al., 2017; Rogge et al., 2023). Arctic Ocean pCO₂ undersaturation is driven by low seawater temperatures, sea ice meltwater input, biological CO₂ uptake during the summer and strong upper ocean stratification (Bates et al., 2006; Takahashi et al., 2009; Fransson et al., 2017). In addition to the variability in the Arctic Ocean's nutrient content and capacity to absorb atmospheric pCO₂ driven by biogeochemical and sea ice processes, physical processes also can lead to changes in the marine nutrient and carbonate system on short time scales. For example, frontal regions are associated with enhanced biological activity, leading to variability in uptake and remineralization rates of nutrients across smaller hydrographic scales

(Eveleth et al., 2014). Tidal currents in regions where horizontal gradients of water masses exist, for example, between the Yermak Plateau and Fram Strait, can also lead to rapid change in the nutrient and carbonate system of the surface ocean on semidiurnal and diurnal time scales and cause polar waters to switch between a CO₂ sink and source multiple times a day (Skogseth et al., 2013; Llanillo et al., 2019; Droste et al., 2022).

8.2.2. Optical properties

The optical properties of the surface waters of the MOSAiC exhibited regional differences between the basins, exemplified by the documented differences in CDOM concentrations, with elevated concentration when in the Transpolar Drift (see Section 4.2). In Arctic waters, CDOM is an important factor of light attenuation in the water column (e.g., Granskog et al., 2007; Hill, 2008; Pavlov et al., 2015) and varies regionally, largely depending on the presence of river water. The presence of river water divides the Eurasian basin into bio-optical provinces (Gonçalves-Araujo et al., 2018), which has implications for light availability for primary producers (e.g., Pavlov et al., 2015), especially in the absence of sea ice. Solar heating of the upper ocean is also affected by the distribution of CDOM (Hill, 2008; Granskog et al., 2015) and could thus affect sea ice melting across regimes.

8.2.3. Ecology

Regional variability in both nutrient concentrations and the optical regime can induce compositional changes to the microbial community, with complex implications for the carbon biogeochemistry. For example, increased vertical transport of nutrients from the deep ventilation observed in the Nansen Basin could lead to a shift from smaller to larger phytoplankton, while increased stratification and warming can lead to opposite trends (Li et al., 2009; Morán et al., 2010). Additionally, hydrographic boundaries can act as physical barriers limiting dispersal, resulting in vertical and biogeographic differences in microbial diversity and community structure among water masses and basins (Galand et al., 2010; Han et al., 2015). During MOSAiC, unique upper water column microbial community compositions were indeed observed when crossing boundaries such as the base of the mixed layer, or when drifting into and out of the Transpolar Drift (Chamberlain, 2023). A key driver in regional differences in Arctic Ocean bacterial communities is the relative proportion of Atlantic water influence, with species composition and ecological function, that is, substrate utilization, responding rapidly to changes in the environmental regime. This connection makes the variability in water masses, for example, the high relative proportion of Atlantic water observed while crossing the Yermak Plateau, a key driver in regional differences of microbial communities (Carter-Gates et al., 2020; Priest et al., 2023). At higher trophic levels, larger boreal species such as fish or squid can enter the Arctic Ocean within the Atlantic Water layer and appear to survive in parts of the central Arctic. During MOSAiC, healthy Atlantic cod were found in the Amundsen Basin, where a deep scattering layer indicated

the presence of living organisms as food supply (Snoeijs-Leijonmalm et al., 2022). In the Nansen Basin, this deep scattering layer was absent and fish and squid abundance decreased. The inflow region of young Atlantic Water near the Yermak Plateau, on the other hand, was characterized by large aggregations of Atlantic fish species (Snoeijs-Leijonmalm et al., 2022).

8.2.4. Sea ice and atmosphere

Oceanic heat, when reaching the surface, affects sea ice growth and melt. During MOSAiC, the sea ice basal growth was found to transition from a rapid to a slower growth rate, when drifting from Amundsen Basin to Nansen Basin (Lei et al., 2022). This change in basal growth rate might be related, to some extent, to the greater vertical heat transport from the Atlantic Water layer in the Nansen Basin, associated with the ventilation conditions (i.e., absence of the halocline; Polyakov et al., 2017). During the melt season, elevated ocean surface temperatures contribute to sea ice melt and small vertical gradients in upper ocean temperature might set different melt rates at, for example, ridge keels (Salganik et al., 2023b). The presence of shallow, strongly stratified meltwater layers also affects sea-ice melt rates (Salganik et al., 2023a; Smith et al., 2023). Indirectly, even atmospheric conditions might be influenced by surface ocean conditions, by affecting the emission of marine aerosol precursors that play an important role in, for example, cloud formation (Schmale et al., 2021).

9. Summary and outlook

For this study, we compiled a quality-controlled dataset of temperature and salinity profiles and derived parameters, with the best available temporal coverage along the whole MOSAiC drift across the Eurasian basin in 2019–2020. Derived core parameters based on this dataset (Table S1; Mieruch, 2023; Schulz et al., 2023b) can be used for interdisciplinary studies aiming to understand interactions between ocean physical properties and a large range of other measurements conducted during MOSAiC. We find that from an ocean perspective, MOSAiC was a transect across the Eurasian basin rather than a time series primarily reflecting a seasonal evolution. Considerable gradients in the surface waters were present, related to the MOSAiC ice camp drifting into and out of the river water-influenced Transpolar Drift in the Amundsen Basin. In the Nansen Basin, high surface salinity and the associated absence of the halocline allowed for a more direct connection and enhanced exchange between the surface and deeper waters of Atlantic origin. Further south, above the Yermak Plateau and in Fram Strait, oceanic conditions were more dynamic, with a pronounced regime shift back into surface waters with a high fraction of terrestrial water when leaving the Yermak Plateau. This spatial variability likely entails large implications for the Arctic Ocean biogeochemistry, ecology, and even sea ice and atmospheric conditions.

The large regional variability encountered during the drift illustrates that MOSAiC results are not representative of the entire Arctic Ocean. Conditions encountered in the

Eurasian deep basins are substantially different from the Amerasian Basin, where the Beaufort Gyre accumulates large amounts of freshwater and Pacific Water is commonly present in the upper water column. Conditions in the basins also deviate from the more variable and energetic continental shelf and slope regions. Furthermore, the observed strong dependence of ocean conditions on the Transpolar Drift pathway, setting surface salinity, stratification and vertical transport, illustrates that a slight deviation in the ice drift path could have restricted the range of sampled conditions. For example, if the drift track had not crossed the Gakkel Ridge and instead had stayed within the cross-Arctic transport pathway of Siberian freshwater, MOSAiC would have missed the ventilation conditions in the Nansen Basin. The pathway of the Transpolar Drift depends on large-scale atmospheric forcing and varies on interannual to decadal timescales (Polyakov et al., 2023). In the period 2007–2021, a positive Arctic Dipole, that is, relatively higher sea level pressure over the Beaufort Sea and Canadian Archipelago and lower sea level pressure over the Siberian Arctic, reinforced both the Beaufort Gyre and shifted the Transpolar Drift path from the Amerasian Basin toward the Lomonosov Ridge. Freshwater of Siberian origin accumulated in the Beaufort Gyre, leading to a stronger salinity stratification in the Amerasian Basin and a weaker stratification in the Eurasian Basin. The underlying atmospheric forcing changes on a timescale of approximately 15 years, and superimposes on climatic trends such as warming Atlantic water and altered freshwater dynamics. For instance, the less pronounced summer sea ice decline since 2007 might originate from reduced ocean heat transport in the presence of stronger stratification in the Amerasian Basin created by the positive Arctic Dipole (Polyakov et al., 2023). The representativeness of MOSAiC results of the annual cycle and for other parts of the Arctic, especially for the biogeochemical and ecological system, needs to be assessed with more observations. Nevertheless, the MOSAiC data provide an important benchmark for detecting future changes in the Eurasian basin.

Future research efforts aiming to monitor climatic trends in the Arctic Ocean need to account for this large interannual and regional variability, which ideally requires long time series from stationary moorings and repeated sections stations, as well as wide temporal and spatial coverage by autonomous drifting buoys and floats. Numerical models will be necessary to extrapolate and scale up observational data, by identifying the spatial extent of distinct oceanographic regimes (e.g., ventilation conditions in the absence of a halocline, as in Polyakov et al., 2017, and observed in the Nansen Basin) in response to seasonal and atmospheric forcing, and process studies will be needed to isolate the respective effect of individual driving mechanisms for ocean variability. The strength of MOSAiC lies in its multidisciplinary approach. MOSAiC observed key parameters simultaneously, including atmospheric forcing, sea ice and ocean conditions, as well as ocean biogeochemistry and ecology, at high temporal sampling frequency and on a range of scales from manned measurements at the central floe and autonomous

platforms in the surrounding area to remote sensing by aircrafts and satellites. This strategy has provided unprecedented means to determine connections within the coupled Arctic system on multiple timescales. Despite the challenges in data interpretation arising from the overlapping timescales and the superposition of spatial and temporal signals inherent to a drift campaign, the large variability of conditions observed during MOSAiC helps us to better understand processes and connections across the coupled system over timescales from hours to months. MOSAiC datasets also provide an unprecedented opportunity for the scientific community to improve the ocean and climate models pivotal to Arctic and Earth system research. Achieving this goal requires dedicated time, effective communication between observational and modeling communities, and adequate funding.

One final aspect we would like to highlight about the value of MOSAiC for the polar and climate research community is the high degree of fruitful scientific collaborations that have been established as a result of this unique experiment. Despite or perhaps because of the complexity of and challenges encountered during the campaign, MOSAiC has created a thriving community that has been working together across disciplines to interpret the collected data, involving an increasing number of early career scientists. Many of the collaborations and partnerships between the international partners have been maintained, and even strengthened and expanded. The project serves as an example of how to foster scientific collaboration and unleash the scientific spirit of a research community. In the end, the true value of MOSAiC may likely be found beyond the experiment itself.

Data accessibility statement

All datasets used in this study are publicly available, in compliance with the MOSAiC data policy. In addition, we published a daily average dataset based on the 2434 temperature and salinity profiles, as outlined in Text S1, and derived parameters, as listed in Table S1, in netCDF format (Schulz et al., 2023b). We also created webODV compliant data files and views (Mieruch, 2023), from which subsets of data can easily be extracted. We strongly advise that future studies using the data presented here also cite the respective original datasets listed below: CO1 GPS buoy: Nicolaus et al. (2021); CTD Polarstern: Tippenhauer et al. (2023b, c); Ocean City CTD: Tippenhauer et al. (2023a, d); MSS: Schulz et al. (2023c); ITPs (including CDOM data): Toole and Krishfield (2016); PG buoy O4: Hopmann et al. (2022); thermosalinograph: Haas et al. (2021); Kanzow et al. (2021); Rex et al. (2021a); Rex et al. (2021b, c); ADCP: Baumann et al. (2021); AOFB: Stanton and Shaw (2023).

Supplemental files

The supplemental files for this article can be found as follows:

Text_S1_SupplementalMaterial.pdf

Acknowledgments

Data used in this manuscript were produced as part of the international Multidisciplinary drifting Observatory for the

Study of the Arctic Climate (MOSAiC) project with the tag MOSAiC20192020 and the Project_ID: AWI_PS122_00. The Ice-Tethered Profiler data were collected and made available by the Ice-Tethered Profiler Program (Krishfield et al., 2008; Toole et al., 2011) based at the Woods Hole Oceanographic Institution (<https://www2.whoi.edu/site/itp/>). We thank all persons involved in the expedition of the Research Vessel *Polarstern* (Knust, 2017) during MOSAiC in 2019–2020 as listed in the MOSAiC extended acknowledgment (Nixdorf et al., 2021). We especially thank everyone involved in the discussion during the Second MOSAiC Science Conference in Boulder, Colorado, which motivated this study. We would also like to thank Daniela Ransby (Pangaea) and Christopher Kracha (Arctic Data Center) for their great support with the data publications. Finally, we like to thank two anonymous reviewers and our editor, Jody Deming, for dedicating their time and for their positive evaluation of our manuscript.

Funding

Financial support for KS was available through the German (BMBF) and UK (NERC) funded PEANUTS-project (grant number 03F0804A) and the NSF funded projects NSF-AccelNet-2020387 and OPP-1936506. ZK, TMB, and IF received funding through the AROMA (Arctic Ocean mixing processes and vertical fluxes of energy and matter) project by the Research Council of Norway (grant no 294396). ZK received funding from the Research Council of Norway through project BREATHE (grant no 325405). MM and MAG were supported by funding from the European Union's Horizon 2020 research and innovation programme under grant agreement No 101003826 via project CRiceS (Climate Relevant interactions and feedbacks: The key role of sea ice and Snow in the polar and global climate system) and the Research Council of Norway through project HAVOC (grant no 280292). MAG also acknowledges support from the Hanse-Wissenschaftskolleg Institute of Advanced Study (Delmenhorst, Germany). MV was supported through the Changing Arctic Ocean (CAO) program, jointly funded by the UKRI Natural Environment Research Council (NERC) and the BMBF, project Advection Pathways of nutrients and key Ecological substances in the ARctic (PEAR) grants NE/R012865/1, NE/R012865/2, and #03V01461. SK and CH were supported by the Swedish Research Council (grant 2018–03859 awarded to CH); participation of SK to MOSAiC was supported by the Swedish Research Polar Secretariat. ESD was supported by the European Union's Horizon 2020 research and innovation programme under grant agreement no. 821001; participation of ESD on MOSAiC was supported by the Natural Environment Research Council (NERC) through the EnvEast Doctoral Training Partnership (grant no. NE/L002582/1) and the UK Department for Business, Energy and Industrial Strategy (BEIS) through the UK Arctic Office. TS and the AOFB measurements are funded by NSF OPP-1723400. GL also gratefully acknowledges financial support from the Ocean Frontier Institute, supported by a Canada First Research Excellence Fund award (grant no. 39291), and from the European Union's Horizon 2020 research and innovation program under a Marie Skłodowska-Curie Postdoctoral Global Fellowship award (grant no. 101023769).

Competing interests

All authors declare that they have no competing interests.

Author contributions

Contributed to conception and design: KS, ZK, CJMH, EJC, MM, IF, CH, MAG.

Contributed to acquisition of data: KS, ZK, MM, DB, CJMH, ESD, MH, EJC, GL, TS, IF, CH, SK, TMB, ST, MAG.

Contributed to analysis and interpretation of data: KS, ZK, MM, DB, CJMH, ESD, EJC, GL, TS, AQ, IF, CH, SK, MV, MAG.

Drafted and/or revised this article: All authors.

Approved the submitted version for publication: All authors.

References

Arrigo, KR, van Dijken, GL. 2015. Continued increases in Arctic Ocean primary production. *Progress in Oceanography* **136**: 60–70. DOI: <https://dx.doi.org/10.1016/j.pocean.2015.05.002>.

Baker, MA, Gibson, CH. 1987. Sampling turbulence in the stratified ocean: Statistical consequences of strong intermittency. *Journal of Physical Oceanography* **17**(10): 1817–1836. DOI: [https://dx.doi.org/10.1175/1520-0485\(1987\)017<1817:STITSO>2.0.CO;2](https://dx.doi.org/10.1175/1520-0485(1987)017<1817:STITSO>2.0.CO;2).

Bates, NR, Mathis, JT. 2009. The Arctic Ocean marine carbon cycle: Evaluation of air-sea CO₂ exchanges, ocean acidification impacts and potential feedbacks. *Biogeosciences* **6**(11): 2433–2459. DOI: <https://dx.doi.org/10.5194/bg-6-2433-2009>.

Bates, NR, Moran, SB, Hansell, DA, Mathis, JT. 2006. An increasing CO₂ sink in the Arctic Ocean due to sea-ice loss. *Geophysical Research Letters* **33**(23). DOI: <https://dx.doi.org/10.1029/2006GL027028>.

Bauch, D, Cherniavskaya, E, Timokhov, L. 2016. Shelf basin exchange along the Siberian continental margin: Modification of Atlantic water and lower halocline water. *Deep Sea Research Part I: Oceanographic Research Papers* **115**: 188–198. DOI: <https://dx.doi.org/10.1016/j.dsri.2016.06.008>.

Bauch, D, van der Loeff, MR, Andersen, N, Torres-Valdes, S, Bakker, K, Abrahamsen, EP. 2011. Origin of freshwater and polynya water in the Arctic Ocean halocline in summer 2007. *Progress in Oceanography* **91**(4): 482–495. DOI: <https://dx.doi.org/10.1016/j.pocean.2011.07.017>.

Baumann, T, Fer, I, Bryhni, H, Peterson, AK, Allerholt, J, Fang, YC, Hoppmann, M, Karam, S, Koenig, Z, Kong, B, Mohrholz, V, Muilwijk, M, Schaffer, J, Schulz, K, Sukhikh, N, Tippenhauer, S. 2021. Under-ice current measurements during MOSAiC from a 75 kHz acoustic Doppler profiler [dataset]. PANGAEA. DOI: <https://dx.doi.org/10.1594/PANGAEA.934792>.

Bouffard, D, Boegman, L. 2013. A diapycnal diffusivity model for stratified environmental flows. *Dynamics of Atmospheres and Oceans* **61–62**: 14–34. DOI: <https://dx.doi.org/10.1016/j.dynatmoce.2013.02.002>.

Bourgain, P, Gascard, JC. 2011. The Arctic Ocean halocline and its interannual variability from 1997 to 2008. *Deep Sea Research Part I: Oceanographic Research Papers* **58**(7): 745–756. DOI: <https://dx.doi.org/10.1016/j.dsri.2011.05.001>.

Boyd, TJ, Steele, M, Muench, RD, Gunn, JT. 2002. Partial recovery of the Arctic Ocean halocline. *Geophysical Research Letters* **29**(14): 2-1–2-4. DOI: <https://dx.doi.org/10.1029/2001GL014047>.

Boyer, TP, Garcia, HE, Locarnini, RA, Zweng, MM, Mishonov, AV, Reagan, JR, Weathers, KA, Baranova, OK, Seidov, D, Smolyar, IV. 2018. World Ocean Atlas 2018. NOAA National Centers for Environmental Information. Available at <https://www.ncei.noaa.gov/archive/acquisition/NCEI-WOA18>. Accessed March 30, 2023.

Carranza, MM, Gille, ST, Franks, PJS, Johnson, KS, Pinkel, R, Girton, JB. 2018. When mixed layers are not mixed. Storm-driven mixing and bio-optical vertical gradients in mixed layers of the Southern Ocean. *Journal of Geophysical Research: Oceans* **123**(10): 7264–7289. DOI: <https://dx.doi.org/10.1029/2018JC014416>.

Carter-Gates, M, Balestreri, C, Thorpe, SE, Cottier, F, Baylay, A, Bibby, TS, Moore, CM, Schroeder, DC. 2020. Implications of increasing Atlantic influence for Arctic microbial community structure. *Scientific Reports* **10**(1): 19262. DOI: <https://dx.doi.org/10.1038/s41598-020-76293-x>.

Chamberlain, EJ. 2023. Microbial contributions to metabolic oxygen turnover in the central Arctic Ocean. ProQuest Dissertations & Theses.

Charette, MA, Kipp, LE, Jensen, LT, Dabrowski, JS, Whitmore, LM, Fitzsimmons, JN, Williford, T, Ulfso, A, Jones, E, Bundy, RM, Vivancos, SM, Pahnke, K, John, SG, Xiang, Y, Hatta, M, Petrova, MV, Heimbürger-Boavida, L-E, Bauch, D, Newton, R, Pasqualini, A, Agather, AM, Amon, RMW, Anderson, RF, Andersson, PS, Benner, R, Bowman, KL, Edwards, RL, Gdaniec, S, Gerrings, LJA, González, AG, Granskog, M, Haley, B, Hammerschmidt, CR, Hansell, DA, Henderson, PB, Kadko, DC, Kaiser, K, Laan, P, Lam, PJ, Lamborg, CH, Levier, M, Li, X, Margolin, AR, Measures, C, Middag, R, Millero, FJ, Moore, WS, Paffrath, R, Planquette, H, Rabe, B, Reader, H, Rember, R, Rijkenberg, MJA, Roy-Barman, M, van der Loeff, MR, Saito, M, Schauer, U, Schlosser, P, Sherrell, RM, Shiller, AM, Slagter, H, Sonke, JE, Stedmon, C, Woosley, RJ, Valk, O, van Ooijen, J, Zhang, R. 2020. The transpolar drift as a source of riverine and shelf-derived trace elements to the central Arctic Ocean. *Journal of Geophysical Research: Oceans* **125**(5): e2019JC015920. DOI: <https://dx.doi.org/10.1029/2019JC015920>.

Dosser, HV, Chanona, M, Waterman, S, Shibley, NC, Timmermans, ML. 2021. Changes in internal wave-driven mixing across the Arctic Ocean: Finescale estimates from an 18-year pan-Arctic record. *Geophysical Research Letters* **48**(8): e2020GL091747. DOI: <https://dx.doi.org/10.1029/2020GL091747>.

Droste, ES, Hoppema, M, González-Dávila, M, Santana-Casiano, JM, Queste, BY, Dall'Olmo, G,

Venables, HJ, Rohardt, G, Ossebaar, S, Schuller, D, Trace-Kleeberg, S, Bakker, DCE. 2022. The influence of tides on the marine carbonate chemistry of a coastal polynya in the south-eastern Weddell Sea. *Ocean Science* **18**(5): 1293–1320. DOI: <https://dx.doi.org/10.5194/os-18-1293-2022>.

Erofeeva, S, Egbert, G. 2020. Arc5km2018: Arctic Ocean Inverse Tide Model on a 5 kilometer grid, 2018 [dataset]. Arctic Data Center. DOI: <https://dx.doi.org/10.18739/A21R6N14K>.

Eveleth, R, Timmermans, M-L, Cassar, N. 2014. Physical and biological controls on oxygen saturation variability in the upper Arctic Ocean. *Journal of Geophysical Research: Oceans* **119**(11): 7420–7432. DOI: <https://dx.doi.org/10.1002/2014JC009816>.

Fer, I. 2009. Weak vertical diffusion allows maintenance of cold halocline in the central Arctic. *Atmospheric and Oceanic Science Letters* **2**(3): 148–152. DOI: <https://dx.doi.org/10.1080/16742834.2009.11446789>.

Fer, I, Baumann, TM, Koenig, Z, Muilwijk, M, Tippenhauer, S. 2022. Upper-ocean turbulence structure and ocean-ice drag coefficient estimates using an ascending microstructure profiler during the MOSAiC drift. *Journal of Geophysical Research: Oceans* **127**(9): e2022JC018751. DOI: <https://dx.doi.org/10.1029/2022JC018751>.

Fer, I, Müller, M, Peterson, AK. 2015. Tidal forcing, energetics, and mixing near the Yermak Plateau. *Ocean Science* **11**(2): 287–304. DOI: <https://dx.doi.org/10.5194/os-11-287-2015>.

Fine, EC, Cole, ST. 2022. Decadal observations of internal wave energy, shear, and mixing in the western Arctic Ocean. *Journal of Geophysical Research: Oceans* **127**(5): e2021JC018056. DOI: <https://dx.doi.org/10.1029/2021JC018056>.

Fong, AA, Hoppe, CJM, Aberle, N, Ashjian, CJ, Assmy, P, Bai, Y, Bakker, DCE, Balmonte, JP, Barry, KR, Bertilsson, S, Boulton, W, Bowman, J, Bozzato, D, Bratbak, G, Buck, M, Campbell, RG, Castellani, G, Chamberlain, EJ, Chen, J, Chierici, M, Cornils, A, Creamean, JM, Damm, E, Dethloff, K, Droste, ES, Ebenhöh, O, Eggers, SL, Engel, A, Flores, H, Fransson, A, Frickenhaus, S, Gardner, J, Gelfman, CE, Granskog, MA, Graeve, M, Havermans, C, Heuzé, C, Hildebrandt, N, Hill, TCJ, Hoppema, M, Immerz, A, Jin, H, Koch, B, Kong, X, Kraberg, A, Lan, M, Lange, BA, Larsen, A, Lebreton, B, Leu, E, Loose, B, Maslowski, W, Mavis, C, Metfies, K, Mock, T, Müller, O, Nicolaus, M, Niehoff, B, Nomura, D, Nöthig, EM, Oggier, M, Oldenburg, E, Olsen, LM, Peekin, I, Perovich, DK, Popa, O, Rabe, B, Ren, J, Rex, M, Rinke, A, Rokitta, S, Rost, B, Sakinan, S, Salganik, E, Schaafsma, FL, Schäfer, H, Schmidt, K, Shoemaker, KM, Shupe, MD, Snoeijs-Leijonmalm, P, Stefels, J, Svenson, A, Tao, R, Torres-Valdés, S, Torstensson, A, Toseland, A, Ulfso, A, Van Leeuwe, MA, Vortkamp, M, Webb, AL, Gradinger, RR. 2023. Overview of the MOSAiC expedition: Ecosystem [preprint]. *Earth arXiv* DOI: <https://dx.doi.org/10.31223/X5P091>.

Forget, G, Campin, JM, Heimbach, P, Hill, CN, Ponte, RM, Wunsch, C. 2015. ECCO version 4: An integrated framework for non-linear inverse modeling and global ocean state estimation. *Geoscientific Model Development* **8**(10): 3071–3104. DOI: <https://dx.doi.org/10.5194/gmd-8-3071-2015>.

Fouest, VL, Babin, M, Tremblay, JÉ. 2013. The fate of riverine nutrients on Arctic shelves. *Biogeosciences* **10**(6): 3661–3677. DOI: <https://dx.doi.org/10.5194/bg-10-3661-2013>.

Fransson, A, Chierici, M, Skjelvan, I, Olsen, A, Assmy, P, Peterson, AK, Spreen, G, Ward, B. 2017. Effects of sea-ice and biogeochemical processes and storms on under-ice water $f\text{CO}_2$ during the winter-spring transition in the high Arctic Ocean: Implications for sea-air CO_2 fluxes. *Journal of Geophysical Research: Oceans* **122**(7): 5566–5587. DOI: <https://dx.doi.org/10.1002/2016JC012478>.

Friis, K, Körtzinger, A, Wallace, DWR. 2003. The salinity normalization of marine inorganic carbon chemistry data. *Geophysical Research Letters* **30**(2). DOI: <https://dx.doi.org/10.1029/2002GL015898>.

Galand, PE, Potvin, M, Casamayor, EO, Lovejoy, C. 2010. Hydrography shapes bacterial biogeography of the deep Arctic Ocean. *The ISME Journal* **4**(4): 564–576. DOI: <https://dx.doi.org/10.1038/ismej.2009.134>.

Gibson, GA, Elliot, S, Clement Kinney, J, Piliouras, A, Jeffery, N. 2022. Assessing the potential impact of river chemistry on Arctic coastal production. *Frontiers in Marine Science* **9**: 738363. DOI: <https://dx.doi.org/10.3389/fmars.2022.738363>.

Gonçalves-Araujo, R, Granskog, MA, Bracher, A, Azetsu-Scott, K, Dodd, PA, Stedmon, CA. 2016. Using fluorescent dissolved organic matter to trace and distinguish the origin of Arctic surface waters. *Scientific Reports* **6**(1): 33978. DOI: <https://dx.doi.org/10.1038/srep33978>.

Gonçalves-Araujo, R, Rabe, B, Peeken, I, Bracher, A. 2018. High colored dissolved organic matter (CDOM) absorption in surface waters of the central-eastern Arctic Ocean: Implications for biogeochemistry and ocean color algorithms. *PLOS One* **13**(1): e0190838. DOI: <https://dx.doi.org/10.1371/journal.pone.0190838>.

Gordó-Vilaseca, C, Stephenson, F, Coll, M, Lavin, C, Costello, MJ. 2023. Three decades of increasing fish biodiversity across the northeast Atlantic and the Arctic Ocean. *Proceedings of the US National Academy of Sciences* **120**(4): e2120869120. DOI: <https://dx.doi.org/10.1073/pnas.2120869120>.

Granskog, MA, Macdonald, RW, Mundy, CJ, Barber, DG. 2007. Distribution, characteristics and potential impacts of chromophoric dissolved organic matter (CDOM) in Hudson Strait and Hudson Bay, Canada. *Continental Shelf Research* **27**(15): 2032–2050. DOI: <https://dx.doi.org/10.1016/j.csr.2007.05.001>.

Granskog, MA, Pavlov, AK, Sagan, S, Kowalcuk, P, Raczkowska, A, Stedmon, CA. 2015. Effect of sea-ice melt on inherent optical properties and

vertical distribution of solar radiant heating in Arctic surface waters. *Journal of Geophysical Research: Oceans* **120**(10): 7028–7039. DOI: <https://dx.doi.org/10.1002/2015JC011087>.

Guthrie, JD, Fer, I, Morison, JH. 2017. Thermohaline staircases in the Amundsen Basin: Possible disruption by shear and mixing. *Journal of Geophysical Research: Oceans* **122**(10): 7767–7782. DOI: <https://dx.doi.org/10.1002/2017JC012993>.

Haas, C, Hoppmann, M, Tippenhauer, S, Rohardt, G. 2021. Continuous thermosalinograph oceanography along RV POLARSTERN cruise track PS122/2. PANGAEA. DOI: <https://dx.doi.org/10.1594/PANGAEA.930024>.

Han, D, Ha, HK, Hwang, CY, Lee, BY, Hur, HG, Lee, YK. 2015. Bacterial communities along stratified water columns at the Chukchi Borderland in the western Arctic Ocean. *Deep Sea Research Part II: Topical Studies in Oceanography* **120**: 52–60. DOI: <https://dx.doi.org/10.1016/j.dsr2.2015.01.018>.

Heuzé, C, Huhn, O, Walter, M, Sukhikh, N, Karam, S, Körtke, W, Vredenborg, M, Bulsiewicz, K, Sütlenfuß, J, Fang, Y-C, Mertens, C, Rabe, B, Tippenhauer, S, Allerholt, J, He, H, Kuhlmeijer, D, Kuznetsov, I, Mallet, M. 2023a. A year of transient tracers chlorofluorocarbon 12 and sulfur hexafluoride, noble gases helium and neon, and tritium in the Arctic Ocean from the MOSAiC expedition (2019–2020) [preprint]. *Earth System Science Data Discussions*. DOI: <https://dx.doi.org/10.5194/essd-2023-232>

Heuzé, C, Zanowski, H, Karam, S, Muilwijk, M. 2023b. The deep Arctic Ocean and Fram Strait in CMIP6 models. *Journal of Climate* **36**(8): 2551–2584. DOI: <https://dx.doi.org/10.1175/JCLI-D-22-0194.1>.

Hill, VJ. 2008. Impacts of chromophoric dissolved organic material on surface ocean heating in the Chukchi Sea. *Journal of Geophysical Research: Oceans* **113**(C7): C07024. DOI: <https://dx.doi.org/10.1029/2007JC004119>.

Hoppmann, M, Kuznetsov, I, Fang, Y-C, Rabe, B. 2022. Processed data of CTD buoys 201901 to 201908 as part of the MOSAiC distributed network. PANGAEA. DOI: <https://dx.doi.org/10.1594/PANGAEA.940320>.

Jakobsson, M, Mayer, LA, Bringensparr, C, Castro, CF, Mohammad, R, Johnson, P, Ketter, T, Accettella, D, Amblas, D, An, L, Arndt, JE, Canals, M, Casamor, JL, Chauché, N, Coakley, B, Danielson, S, Demarte, M, Dickson, ML, Dorschel, B, Dowdeswell, JA, Dreutter, S, Fremand, AC, Gallant, D, Hall, JK, Hehemann, L, Hodnesdal, H, Hong, J, Ivaldi, R, Kane, E, Klaucke, I, Krawczyk, DW, Kristoffersen, Y, Kuipers, BR, Millan, R, Masetti, G, Morlighem, M, Noormets, R, Prescott, MM, Rebesco, M, Rignot, E, Semiletov, I, Tate, AJ, Travaglini, P, Velicogna, I, Weatherall, P, Weinrebe, W, Willis, JK, Wood, M, Zarayskaya, Y, Zhang, T, Zimmerman, M, Zinglersen, KB. 2020. The International Bathymetric Chart of the Arctic Ocean version 4.0. *Scientific Data* **7**(1): 176. DOI: <https://dx.doi.org/10.1038/s41597-020-0520-9>.

Janout, MA, Hölemann, J, Laukert, G, Smirnov, A, Krumpen, T, Bauch, D, Timokhov, L. 2020. On the variability of stratification in the freshwater-influenced Laptev Sea Region. *Frontiers in Marine Science* **7**: 543489. DOI: <https://dx.doi.org/10.3389/fmars.2020.543489>.

Juranek, LW. 2022. Changing biogeochemistry of the Arctic Ocean: Surface nutrient and CO₂ cycling in a warming, melting north. *Oceanography* **35**(3/4): 144–155. DOI: <https://dx.doi.org/10.5670/oceanog.2022.120>.

Kanzow, T, Hoppmann, M, Tippenhauer, S, Rohardt, G. 2021. Continuous thermosalinograph oceanography along RV POLARSTERN cruise track PS122/3. PANGAEA. DOI: <https://dx.doi.org/10.1594/PANGAEA.930026>

Karam, S, Heuzé, C, Hoppmann, M, de Steur, L. 2024. Continued warming of deep waters in Fram Strait. *EGUsphere* **2024**: 1–23. DOI: <https://dx.doi.org/10.5194/egusphere-2024-458>.

Karam, S, Heuzé, C, Müller, V, Zheng, Y. 2023. Recirculation of Canada basin deep water in the Amundsen Basin, Arctic. *Journal of Physical Oceanography* **53**(11): 2559–2574. DOI: <https://dx.doi.org/10.1175/JPO-D-22-0252.1>.

Karcher, M, Smith, JN, Kauker, F, Gerdes, R, Smethie, WM Jr. 2012. Recent changes in Arctic Ocean circulation revealed by iodine-129 observations and modeling. *Journal of Geophysical Research: Ocean* **117**(C8): C08007. DOI: <https://dx.doi.org/10.1029/2011JC007513>.

Kawaguchi, Y, Koenig, Z, Nomura, D, Hoppmann, M, Inoue, J, Fang, YC, Schulz, K, Gallagher, M, Katilein, C, Nicolaus, M, Rabe, B. 2022. Turbulent mixing during late summer in the ice–ocean boundary layer in the central Arctic Ocean: Results from the MOSAiC expedition. *Journal of Geophysical Research: Oceans* **127**(8): e2021JC017975. DOI: <https://dx.doi.org/10.1029/2021JC017975>.

Kim, Y-H, Min, S-K, Gillett, NP, Notz, D, Malinina, E. 2023. Observationally-constrained projections of an ice-free Arctic even under a low emission scenario. *Nature Communications* **14**(1): 3139. DOI: <https://dx.doi.org/10.1038/s41467-023-38511-8>.

Knust, R. 2017. Polar research and supply vessel POLARSTERN operated by the Alfred-Wegener-Institute. *Journal of Large-Scale Research Facilities* **3**: A119. DOI: <https://dx.doi.org/10.17815/jlsrf-3-163>.

Kong, X. 2022. Molecular and optical characterization of dissolved organic matter in the Central Arctic Ocean [PhD thesis]. Bremen, Germany: University of Bremen: 159. DOI: <https://doi.org/10.26092/elib/1981>.

Korhonen, M, Rudels, B, Marnela, M, Wisotzki, A, Zhao, J. 2013. Time and space variability of freshwater content, heat content and seasonal ice melt in the Arctic Ocean from 1991 to 2011. *Ocean Science* **9**(6): 1015–1055. DOI: <https://dx.doi.org/10.5194/osd-9-2621-2012>.

Krishfield, R, Toole, J, Proshutinsky, A, Timmermans, M-L. 2008. Automated ice-tethered profilers for sea-water observations under pack ice in all seasons.

Journal of Atmospheric and Oceanic Technology **25**(11): 2091–2105. DOI: <https://dx.doi.org/10.1175/2008JTECHO587.1>.

Krumpen, T, Belter, HJ, Boetius, A, Damm, E, Haas, C, Hendricks, S, Nicolaus, M, Nöthig, EM, Paul, S, Peeken, I, Ricker, R, Stein, R. 2019. Arctic warming interrupts the transpolar drift and affects long-range transport of sea ice and ice-rafted matter. *Scientific Reports* **9**(1): 5459. DOI: <https://dx.doi.org/10.1038/s41598-019-41456-y>.

Kwok, R. 2018. Arctic sea ice thickness, volume, and multiyear ice coverage: Losses and coupled variability (1958–2018). *Environmental Research Letters* **13**(10): 105005. DOI: <https://dx.doi.org/10.1088/1748-9326/aae3ec>.

Lannuzel, D, Tedesco, L, Van Leeuwe, M, Campbell, K, Flores, H, Delille, B, Miller, L, Stefels, J, Assmy, P, Bowman, J, Brown, K, Castellani, G, Chierici, M, Crabeck, O, Damm, E, Else, B, Fransson, A, Fripiat, F, Geilfus, N-X, Jacques, C, Jones, E, Kaartokallio, H, Kotovitch, M, Meiners, K, Moreau, S, Nomura, D, Peeken, I, Rintala, JM, Steiner, N, Tison, JL, Vancoppenolle, M, Van der Linden, F, Vichi, M, Wongpan, P. 2020. The future of Arctic sea-ice biogeochemistry and ice-associated ecosystems. *Nature Climate Change* **10**(11): 983–992. DOI: <https://dx.doi.org/10.1038/s41558-020-00940-4>.

Laukert, G, Frank, M, Bauch, D, Hathorne, EC, Rabe, B, von Appen, W-J, Wegner, C, Zieringer, M, Kassens, H. 2017. Ocean circulation and freshwater pathways in the Arctic Mediterranean based on a combined Nd isotope, REE and oxygen isotope section across Fram Strait. *Geochimica et Cosmochimica Acta* **202**: 285–309. DOI: <https://dx.doi.org/10.1016/j.gca.2016.12.028>.

Laukert, G, Grasse, P, Novikhin, A, Povazhnyi, V, Doering, K, Hölemann, J, Janout, M, Bauch, D, Kassens, H, Frank, M. 2022. Nutrient and silicon isotope dynamics in the Laptev Sea and implications for nutrient availability in the transpolar drift. *Global Biogeochemical Cycles* **36**(9): e2022GB007316. DOI: <https://dx.doi.org/10.1029/2022GB007316>.

Laukert, G, Makhotin, M, Petrova, MV, Frank, M, Hathorne, EC, Bauch, D, Böning, P, Kassens, H. 2019. Water mass transformation in the Barents Sea inferred from radiogenic neodymium isotopes, rare earth elements and stable oxygen isotopes. *Chemical Geology* **511**: 416–430. DOI: <https://dx.doi.org/10.1016/j.chemgeo.2018.10.002>.

Lei, R, Cheng, B, Hoppmann, M, Zhang, F, Zuo, G, Hutchings, JK, Lin, L, Lan, M, Wang, H, Regnery, J, Krumpen, T, Haapala, J, Rabe, B, Perovich, DK, Nicolaus, M. 2022. Seasonality and timing of sea ice mass balance and heat fluxes in the Arctic transpolar drift during 2019–2020. *Elementa Science of the Anthropocene* **10**(1): 000089. DOI: <https://dx.doi.org/10.1525/elementa.2021.000089>.

Lenn, YD, Wiles, P, Torres-Valdes, S, Abrahamsen, E, Rippeth, T, Simpson, J, Bacon, S, Laxon, S, Polyakov, I, Ivanov, V, Kirillov, S. 2009. Vertical mixing at intermediate depths in the Arctic boundary current. *Geophysical Research Letters* **36**(5). DOI: <https://dx.doi.org/10.1029/2008GL036792>.

Li, WK, McLaughlin, FA, Lovejoy, C, Carmack, EC. 2009. Smallest algae thrive as the Arctic Ocean freshens. *Science* **326**(5952): 539. DOI: <https://dx.doi.org/10.1126/science.1179798>.

Llanillo, P, Aiken, CM, Cordero, RR, Damiani, A, Sepúlveda, E, Fernández-Gómez, B. 2019. Oceanographic variability induced by tides, the intraseasonal cycle and warm subsurface water intrusions in Maxwell Bay, King George Island (West-Antarctica). *Scientific Reports* **9**(1): 18571. DOI: <https://dx.doi.org/10.1038/s41598-019-54875-8>.

Locarnini, R, Mishonov, A, Baranova, O, Boyer, T, Zweng, M, Garcia, H, Reagan, J, Seidov, D, Weathers, K, Paver, C, Smolyar, I. 2018. World Ocean Atlas 2018, Volume 1: Temperature. A. Mishonov Technical Ed.; NOAA Atlas NESDIS 81.

Marnela, M, Rudels, B, Gosczko, I, Beszczynska-Möller, A, Schauer, U. 2016. Fram Strait and Greenland Sea transports, water masses, and water mass transformations 1999–2010 (and beyond). *Journal of Geophysical Research: Oceans* **121**(4): 2314–2346. DOI: <https://dx.doi.org/10.1002/2015JC011312>.

McDougall, TJ, Barker, PM. 2011. Getting started with TEOS-10 and the Gibbs Seawater (GSW) oceanographic toolbox. SCOR/IAPSO WG127: 1–28.

McPhee, M. 2008. *Air-ice-ocean interaction: Turbulent ocean boundary layer exchange processes*. Dordrecht, the Netherlands: Springer Science & Business Media.

Meyer, A, Fer, I, Sundfjord, A, Peterson, AK. 2017a. Mixing rates and vertical heat fluxes north of Svalbard from Arctic winter to spring. *Journal of Geophysical Research: Oceans* **122**(6): 4569–4586. DOI: <https://dx.doi.org/10.1002/2016JC012441>.

Meyer, A, Sundfjord, A, Fer, I, Provost, C, Villacíeros Robineau, N, Koenig, Z, Onarheim, IH, Smedsrød, LH, Duarte, P, Dodd, PA, Graham, RM, Schmidtko, S, Kauko, HM. 2017b. Winter to summer oceanographic observations in the Arctic Ocean north of Svalbard. *Journal of Geophysical Research: Oceans* **122**(8): 6218–6237. DOI: <https://dx.doi.org/10.1002/2016JC012391>.

Mieruch, S. 2023. Smieruch/mosaic_hydrographic_core_parameters: Initial release. Zenodo. DOI: <https://doi.org/10.5281/zenodo.8304184>.

Mieruch, S, Schlitzer, R. 2023. smieruch/webody: webODV v1.0.0. Zenodo. DOI: <https://dx.doi.org/10.5281/zenodo.8241241>.

Morán, XAG, López-Urrutia, Á, Calvo-Díaz, A, Li, WKW. 2010. Increasing importance of small phytoplankton in a warmer ocean. *Global Change Biology* **16**(3): 1137–1144. DOI: <https://doi.org/10.1111/j.1365-2486.2009.01960.x>.

Mysak, LA. 2001. Patterns of Arctic circulation. *Science* **293**(5533): 1269–1270. DOI: <https://dx.doi.org/10.1126/science.1064217>.

Nguyen, AT, Pillar, H, Ocaña, V, Biggeli, A, Smith, TA, Heimbach, P. 2021. The Arctic Subpolar gyre sTate Estimate: Description and assessment of a data-constrained, dynamically consistent ocean-sea ice estimate for 2002–2017. *Journal of Advances in Modeling Earth Systems* **13**(5): e2020MS002398. DOI: <https://dx.doi.org/10.1029/2020MS002398>.

Nicolaus, M, Perovich, DK, Spreen, G, Granskog, MA, von Albedyll, L, Angelopoulos, M, Anhaus, P, Arndt, S, Belter, HJ, Bessonov, V, Birnbaum, G, Brauchle, J, Calmer, R, Cardellach, E, Cheng, B, Clemens-Sewall, D, Dadic, R, Damm, E, de Boer, G, Demir, O, Dethloff, K, Divine, DV, Fong, AA, Fons, S, Frey, MM, Fuchs, N, Gabarró, C, Gerland, S, Goessling, HF, Gradinger, R, Haapala, J, Haas, C, Hamilton, J, Hannula, HR, Hendricks, S, Herber, A, Heuzé, C, Hoppmann, M, Høyland, KV, Huntemann, M, Hutchings, JK, Hwang, B, Itkin, P, Jacobi, HW, Jaggi, M, Jutila, A, Kaleschke, L, Katlein, C, Kolabutin, N, Krampe, D, Kristensen, SS, Krumpen, T, Kurtz, N, Lampert, A, Lange, BA, Lei, R, Light, B, Linhardt, F, Liston, GE, Loose, B, Macfarlane, AR, Mahmud, M, Matero, IO, Maus, S, Morgenstern, A, Naderpour, R, Nandan, V, Niubom, A, Oggier, M, Oppelt, N, Pätzold, F, Perron, C, Petrovsky, T, Pirazzini, R, Polashenski, C, Rabe, B, Raphael, IA, Regnery, J, Rex, M, Ricker, R, Riemann-Campe, K, Rinke, A, Rohde, J, Salganik, E, Scharien, RK, Schiller, M, Schneebeli, M, Semmling, M, Shimanchuk, E, Shupe, MD, Smith, MM, Smolyanitsky, V, Sokolov, V, Stanton, T, Stroeve, J, Thielke, L, Timofeeva, A, Tonboe, RT, Tavri, A, Tsamados, M, Wagner, DN, Watkins, D, Webster, M, Wendisch, M. 2022. Overview of the MOSAiC expedition: Snow and sea ice. *Elementa: Science of the Anthropocene* **10**(1): 000046. DOI: <https://dx.doi.org/10.1525/elementa.2021.000046>.

Nicolaus, M, Riemann-Campe, K, Bliss, A, Hutchings, JK, Granskog, MA, Haas, C, Hoppmann, M, Kanzow, T, Krishfield, RA, Lei, R, Rex, M, Li, T, Rabe, B. 2021. Drift trajectories of the main sites of the distributed network of MOSAiC 2019/2020. PANGAEA. DOI: <https://dx.doi.org/10.1594/PANGAEA.937204>.

Nixdorf, U, Dethloff, K, Rex, M, Shupe, M, Sommerfeld, A, Perovich, DK, Nicolaus, M, Heuzé, C, Rabe, B, Loose, B, Damm, E, Gradinger, R, Fong, A, Maslowski, W, Rinke, A, Kwok, R, Spreen, G, Wendisch, M, Herber, A, Hirsekorn, M, Mohaupt, V, Frickenhaus, S, Immerz, A, Weiss-Tuider, K, König, B, Mengedoht, D, Regnery, J, Gerchow, P, Ransby, D, Krumpen, T, Morgenstern, A, Haas, C, Kanzow, T, Rack, FR, Saitzev, V, Sokolov, V, Makarov, A, Schwarze, S, Wunderlich, T, Wurr, K, Boetius, A. 2021. MOSAiC Extended Acknowledgement. Zenodo. DOI: <https://dx.doi.org/10.5281/zenodo.5541624>.

Nomura, D, Kawaguchi, Y, Webb, AL, Li, Y, Dall'osto, M, Schmidt, K, Droste, ES, Chamberlain, EJ, Kolabutin, N, Shimanchuk, E, Hoppmann, M, Gallagher, MR, Meyer, H, Mellat, M, Bauch, D, Gabarró, C, Smith, MM, Inoue, J, Damm, E, Delille, B. 2023. Meltwater layer dynamics in a central Arctic lead: Effects of lead width, re-freezing, and mixing during late summer. *Elementa: Science of the Anthropocene* **11**(1). DOI: <https://dx.doi.org/10.1525/elementa.2022.00102>.

Paffrath, R, Laukert, G, Bauch, D, van der Loeff, MR, Pahnke, K. 2021. Separating individual contributions of major Siberian rivers in the Transpolar Drift of the Arctic Ocean. *Scientific Reports* **11**: 8216. DOI: <https://dx.doi.org/10.1038/s41598-021-86948-y>.

Pavlov, AK, Granskog, MA, Stedmon, CA, Ivanov, BV, Hudson, SR, Falk-Petersen, S. 2015. Contrasting optical properties of surface waters across the Fram Strait and its potential biological implications. *Journal of Marine Systems* **143**: 62–72. DOI: <https://dx.doi.org/10.1016/j.jmarsys.2014.11.001>.

Peralta-Ferriz, C, Woodgate, RA. 2015. Seasonal and interannual variability of pan-Arctic surface mixed layer properties from 1979 to 2012 from hydrographic data, and the dominance of stratification for multiyear mixed layer depth shoaling. *Progress in Oceanography* **134**: 19–53. DOI: <https://dx.doi.org/10.1016/j.pocean.2014.12.005>.

Perovich, D, Raphael, I, Moore, R, Clemens-Sewall, D, Lei, R, Sledd, A, Polashenski, C. 2023. Sea ice heat and mass balance measurements from four autonomous buoys during the MOSAiC drift campaign. *Elementa: Science of the Anthropocene* **11**(1). DOI: <https://dx.doi.org/10.1525/elementa.2023.00017>.

Polyakov, IV, Ingvaldsen, RB, Pnyushkov, AV, Bhatt, US, Francis, JA, Janout, M, Kwok, R, Skagseth, Ø. 2023. Fluctuating Atlantic inflows modulate Arctic atlantification. *Science* **381**(6661): 972–979. DOI: <https://dx.doi.org/10.1126/science.adh5158>.

Polyakov, IV, Pnyushkov, AV, Alkire, MB, Ashik, IM, Baumann, TM, Carmack, EC, Gosczko, I, Guthrie, J, Ivanov, VV, Kanzow, T, Krishfield, R, Kwok, R, Sundfjord, A, Morison, J, Rember, R, Yulin, A. 2017. Greater role for Atlantic inflows on sea-ice loss in the Eurasian Basin of the Arctic Ocean. *Science* **356**(6335): 285–291. DOI: <https://dx.doi.org/10.1126/science.aai8204>.

Polyakov, IV, Rippeth, TP, Fer, I, Alkire, MB, Baumann, TM, Carmack, EC, Ingvaldsen, R, Ivanov, VV, Janout, M, Lind, S, Padman, L, Pnyushkov, AV, Rember, R. 2020a. Weakening of cold halocline layer exposes sea ice to oceanic heat in the eastern Arctic Ocean. *Journal of Climate* **33**(18): 8107–8123. DOI: <https://dx.doi.org/10.1175/JCLI-D-19-0976.1>.

Polyakov, IV, Rippeth, TP, Fer, I, Baumann, TM, Carmack, EC, Ivanov, VV, Janout, M, Padman, L, Pnyushkov, AV, Rember, R. 2020b. Intensification of near-surface currents and shear in the Eastern Arctic Ocean. *Geophysical Research Letters* **47**(16): e2020GL089469. DOI: <https://dx.doi.org/10.1029/2020GL089469>.

Priest, T, von Appen, W-J, Oldenburg, E, Popa, O, Torres-Valdés, S, Bienhold, C, Metfies, K, Boulton, W, Mock, T, Fuchs, BM, Amann, R, Boetius,

A, Wietz, M. 2023. Atlantic water influx and sea-ice cover drive taxonomic and functional shifts in Arctic marine bacterial communities. *The ISME Journal* **17**(10): 1612–1625. DOI: <https://dx.doi.org/10.1038/s41396-023-01461-6>.

Rabe, B, Heuzé, C, Regnery, J, Aksenov, Y, Allerholt, J, Athanase, M, Bai, Y, Basque, C, Bauch, D, Baumann, TM, Chen, D, Cole, ST, Craw, L, Davies, A, Damm, E, Dethloff, K, Divine, DV, Doglioni, F, Ebert, F, Fang, YC, Fer, I, Fong, AA, Gradinger, R, Granskog, MA, Graupner, R, Haas, C, He, H, He, Y, Hoppmann, M, Janout, M, Kadko, D, Kanzow, T, Karam, S, Kawaguchi, Y, Koenig, Z, Kong, B, Krishfield, RA, Krumpen, T, Kuhlmeijer, D, Kuznetsov, I, Lan, M, Laukert, G, Lei, R, Li, T, Torres-Valdés, S, Lin, L, Lin, L, Liu, H, Liu, N, Loose, B, Ma, X, MacKay, R, Mallet, M, Mallett, RDC, Maslowski, W, Mertens, C, Mohrholz, V, Muilwijk, M, Nicolaus, M, O'Brien, JK, Perovich, D, Ren, J, Rex, M, Ribeiro, N, Rinke, A, Schaffer, J, Schuffenhauer, I, Schulz, K, Shupe, MD, Shaw, W, Sokolov, V, Sommerfeld, A, Spreen, G, Stanton, T, Stephens, M, Su, J, Sukhikh, N, Sundfjord, A, Thomisch, K, Tippenhauer, S, Toole, JM, Vredenborg, M, Walter, M, Wang, H, Wang, L, Wang, Y, Wendisch, M, Zhao, J, Zhou, M, Zhu, J. 2022. Overview of the MOSAiC expedition: Physical oceanography. *Elementa: Science of the Anthropocene* **10**(1): 00062. DOI: <https://dx.doi.org/10.1525/elementa.2021.00062>.

Randelhoff, A, Holding, J, Janout, M, Sejr, MK, Babin, M, Tremblay, J-E, Alkire, MB. 2020. Pan-Arctic ocean primary production constrained by turbulent nitrate fluxes. *Frontiers in Marine Science* **7**: 150. DOI: <https://dx.doi.org/10.3389/fmars.2020.00150>.

Rantanen, M, Karpechko, AY, Lippinen, A, Nordling, K, Hyvärinen, O, Ruosteenoja, K, Vihma, T, Laaksonen, A. 2022. The Arctic has warmed nearly four times faster than the globe since 1979. *Communications Earth & Environment* **3**(1): 168. DOI: <https://dx.doi.org/10.1038/s43247-022-00498-3>.

Rex, M, Hoppmann, M, Tippenhauer, S, Rohardt, G. 2021a. Continuous thermosalinograph oceanography along RV POLARSTERN cruise track PS122/1. PANGAEA. DOI: <https://dx.doi.org/10.1594/PANGAEA.930023>.

Rex, M, Hoppmann, M, Tippenhauer, S, Rohardt, G. 2021b. Continuous thermosalinograph oceanography along RV POLARSTERN cruise track PS122/4. PANGAEA. DOI: <https://dx.doi.org/10.1594/PANGAEA.930027>.

Rex, M, Hoppmann, M, Tippenhauer, S, Rohardt, G. 2021c. Continuous thermosalinograph oceanography along RV POLARSTERN cruise track PS122/5. PANGAEA. DOI: <https://dx.doi.org/10.1594/PANGAEA.930028>.

Rippeth, TP, Lincoln, BJ, Lenn, Y-D, Green, JM, Sundfjord, A, Bacon, S. 2015. Tide-mediated warming of Arctic halocline by Atlantic heat fluxes over rough topography. *Nature Geoscience* **8**(3): 191–194. DOI: <https://dx.doi.org/10.1038/ngeo2350>.

Rogge, A, Janout, M, Loginova, N, Trudnowska, E, Hörstmann, C, Wekerle, C, Oziel, L, Schourup-Kristensen, V, Ruiz-Castillo, E, Schulz, K, Povazhnyy, VV, Iversen, MH, Waite, AM. 2023. Carbon dioxide sink in the Arctic Ocean from cross-shelf transport of dense Barents Sea water. *Nature Geoscience* **16**(1): 82–88. DOI: <https://dx.doi.org/10.1038/s41561-022-01069-z>.

Rudels, B. 2009. *Arctic Ocean Circulation*. Boston, MA: Academic Press.

Rudels, B. 2012. Arctic Ocean circulation and variability-advection and external forcing encounter constraints and local processes. *Ocean Science* **8**(2): 261–286. DOI: <https://dx.doi.org/10.5194/os-8-261-2012>.

Rudels, B. 2015. Arctic Ocean circulation, processes and water masses: A description of observations and ideas with focus on the period prior to the International Polar Year 2007–2009. *Progress in Oceanography* **132**: 22–67. DOI: <https://dx.doi.org/10.1016/j.pocean.2013.11.006>.

Rudels, B, Hainbucher, D. 2020. On the formation and spreading of thermohaline intrusions in the Arctic Ocean. *Geophysica* **55**(1–2): 23–59.

Salganik, E, Katlein, C, Lange, BA, Matero, I, Lei, R, Fong, AA, Fons, SW, Divine, D, Oggier, M, Castellani, G, Bozzato, D, Chamberlain, EJ, Hoppe, CJM, Müller, O, Gardner, J, Rinke, A, Pereira, PS, Ulfssbo, A, Marsay, C, Webster, MA, Maus, S, Høyland, KV, Granskog, MA. 2023a. Temporal evolution of under-ice meltwater layers and false bottoms and their impact on summer Arctic sea ice mass balance. *Elementa: Science of the Anthropocene* **11**(1): 00035. DOI: <https://dx.doi.org/10.1525/elementa.2022.00035>.

Salganik, E, Lange, BA, Katlein, C, Matero, I, Anhaus, P, Muilwijk, M, Høyland, KV, Granskog, MA. 2023b. Observations of preferential summer melt of Arctic sea-ice ridge keels from repeated multibeam sonar surveys. *The Cryosphere* **17**(11): 4873–4887. DOI: <https://dx.doi.org/10.5194/tc-17-4873-2023>.

Schauer, U, Muench, RD, Rudels, B, Timokhov, L. 1997. Impact of eastern Arctic shelf waters on the Nansen Basin intermediate layers. *Journal of Geophysical Research: Oceans* **102**(C2): 3371–3382. DOI: <https://dx.doi.org/10.1029/96JC03366>.

Schmale, J, Zieger, P, Ekman, AM. 2021. Aerosols in current and future Arctic climate. *Nature Climate Change* **11**(2): 95–105. DOI: <https://dx.doi.org/10.1038/s41558-020-00969-5>.

Schmidtko, S, Johnson, GC, Lyman, JM. 2013. MIMOC: A global monthly isopycnal upper-ocean climatology with mixed layers. *Journal of Geophysical Research: Oceans* **118**(4): 1658–1672. DOI: <https://dx.doi.org/10.1002/jgrc.20122>.

Schulz, K, Janout, M, Lenn, YD, Ruiz-Castillo, E, Polyakov, I, Mohrholz, V, Tippenhauer, S, Reeve, KA, Hölemann, J, Rabe, B, Vredenborg, M. 2021. On the along-slope heat loss of the Boundary Current in

the Eastern Arctic Ocean. *Journal of Geophysical Research: Oceans* **126**(2): e2020JC016375. DOI: <https://dx.doi.org/10.1029/2020JC016375>.

Schulz, K, Kadko, D, Mohrholz, V, Stephens, M, Fer, I. 2023a. Winter vertical diffusion rates in the Arctic Ocean, estimated from ^{7}Be measurements and dissipation rate profiles. *Journal of Geophysical Research: Oceans* **128**(2): e2022JC019197. DOI: <https://dx.doi.org/10.1029/2022JC019197>.

Schulz, K, Koenig, Z, Muilwijk, M. 2023b. The Eurasian Arctic Ocean along the MOSAiC drift (2019–2020): Core hydrographic parameters. Arctic Data Center. DOI: <https://doi.org/10.18739/A21J9790B>.

Schulz, K, Lincoln, B, Povazhnyy, V, Rippeth, T, Lenn, Y-D, Janout, M, Alkire, M, Scannell, B, Torres-Valdés, S. 2022a. Increasing nutrient fluxes and mixing regime changes in the eastern Arctic Ocean. *Geophysical Research Letters* **49**(5): e2021GL096152. DOI: <https://dx.doi.org/10.1029/2021GL096152>.

Schulz, K, Mohrholz, V, Fer, I, Janout, M, Hoppmann, M, Schaffer, J, Koenig, Z. 2022b. A full year of turbulence measurements from a drift campaign in the Arctic Ocean 2019–2020. *Scientific Data* **9**(1): 472. DOI: <https://dx.doi.org/10.1038/s41597-022-01574-1>.

Schulz, K, Mohrholz, V, Fer, I, Janout, MA, Hoppmann, M, Schaffer, J, Koenig, Z, Rabe, B, Heuzé, C, Regnery, J, Allerholt, J, Fang, YC, He, H, Kanzow, T, Karam, S, Kuznetsov, I, Kong, B, Liu, H, Muilwijk, M, Schuffenhauer, I, Sukhikh, N, Sundfjord, A, Tippenhauer, S. 2023c. Turbulent microstructure profile (MSS) measurements from the MOSAiC drift, Arctic Ocean, version 2. PANGAEA. DOI: <https://doi.pangaea.de/10.1594/PANGAEA.961798>.

Schuster, U, McKinley, GA, Bates, N, Chevallier, F, Doney, SC, Fay, AR, González-Dávila, M, Gruber, N, Jones, S, Krijnen, J, Landschützer, P, Lefèvre, N, Manizza, M, Mathis, J, Metzl, N, Olsen, A, Rios, AF, Rödenbeck, C, Santana-Casiano, JM, Takahashi, T, Wanninkhof, R, Watson, AJ. 2013. An assessment of the Atlantic and Arctic sea–air CO_2 fluxes, 1990–2009. *Biogeosciences* **10**(1): 607–627. DOI: <https://dx.doi.org/10.5194/bg-10-607-2013>.

Shaw, WJ, Stanton, TP. 2014. Vertical diffusivity of the Western Arctic Ocean halocline. *Journal of Geophysical Research: Oceans* **119**(8): 5017–5038. DOI: <https://dx.doi.org/10.1002/2013JC009598>.

Shibley, NC, Timmermans, M-L, Carpenter, JR, Toole, JM. 2017. Spatial variability of the Arctic Ocean's double-diffusive staircase. *Journal of Geophysical Research: Oceans* **122**(2): 980–994. DOI: <https://dx.doi.org/10.1002/2016JC012419>.

Shupe, MD, Rex, M, Blomquist, B, Persson, POG, Schmale, J, Uttal, T, Althausen, D, Angot, H, Archer, S, Bariteau, L, Beck, I, Bilberry, J, Bucci, S, Buck, C, Boyer, M, Brasseur, Z, Brooks, IM, Calmer, R, Cassano, J, Castro, V, Chu, D, Costa, D, Cox, CJ, Creamean, J, Crewell, S, Dahlke, S, Damm, E, de Boer, G, Deckelmann, H, Dethloff, K, Dütsch, M, Ebelt, K, Ehrlich, A, Ellis, J, Engelmann, R, Fong, AA, Frey, MM, Gallagher, MR, Ganzeveld, L, Gradinger, R, Graeser, J, Greenamyer, V, Griesche, H, Griffiths, S, Hamilton, J, Heinemann, G, Helmig, D, Herber, A, Heuzé, C, Hofer, J, Houchens, T, Howard, D, Inoue, J, Jacobi, HW, Jaiser, R, Jokinen, T, Jourdan, O, Jozef, G, King, W, Kirchgaessner, A, Klingebiel, M, Krassovski, M, Krumpen, T, Lampert, A, Landing, W, Laurila, T, Lawrence, D, Lonardi, M, Loose, B, Lüpkes, C, Maahn, M, Macke, A, Maslowski, W, Marsay, C, Maturilli, M, Mech, M, Morris, S, Moser, M, Nicolaus, M, Ortega, P, Osborn, J, Pätzold, F, Perovich, DK, Petäjä, T, Pilz, C, Pirazzini, R, Posman, K, Powers, H, Pratt, KA, Preußer, A, Quéléver, L, Radenz, M, Rabe, B, Rinke, A, Sachs, T, Schulz, A, Siebert, H, Silva, T, Solomon, A, Sommerfeld, A, Spreen, G, Stephens, M, Stohl, A, Svensson, G, Uin, J, Viegas, J, Voigt, C, von der Gathen, P, Wehner, B, Welker, JM, Wendisch, M, Werner, M, Xie, Z, Yue, F. 2022. Overview of the MOSAiC expedition: Atmosphere. *Elementa: Science of the Anthropocene* **10**(1): 00060. DOI: <https://doi.org/10.1525/elementa.2021.00060>.

Sirevaag, A, Fer, I. 2012. Vertical heat transfer in the Arctic Ocean: The role of double-diffusive mixing. *Journal of Geophysical Research: Oceans* **117**(C7). DOI: <https://dx.doi.org/10.1029/2012JC007910>.

Skogseth, R, McPhee, MG, Nilsen, F, Smedsrød, LH. 2013. Creation and tidal advection of a cold salinity front in Storfjorden: 1. Polynya dynamics. *Journal of Geophysical Research: Oceans* **118**(7): 3278–3291. DOI: <https://dx.doi.org/10.1002/jgrc.20231>.

Smedsrød, LH, Esau, I, Ingvaldsen, RB, Eldevik, T, Hauge, PM, Li, C, Lien, VS, Olsen, A, Omar, AM, Otterå, OH, Risebrobakken, B, Sandø, AB, Semenov, VA, Sorokina, SA. 2013. The role of the Barents Sea in the Arctic climate system. *Reviews of Geophysics* **51**(3): 415–449. DOI: <https://dx.doi.org/10.1002/rog.20017>.

Smethie W Jr, Chipman, D, Swift, J, Koltermann, K. 1988. Chlorofluoromethanes in the Arctic Mediterranean seas: Evidence for formation of bottom water in the Eurasian Basin and deep-water exchange through Fram Strait. *Deep Sea Research Part A Oceanographic Research Papers* **35**(3): 347–369. DOI: [https://dx.doi.org/10.1016/0198-0149\(88\)90015-5](https://dx.doi.org/10.1016/0198-0149(88)90015-5).

Smith, MM, Angot, H, Chamberlain, EJ, Drost, E, Karam, S, Muilwijk, M, Webb, AL, Archer, SD, Beck, I, Blomquist, BW, Bowman, J, Boyer, M, Bozzato, D, Chierici, M, Creamean, J, D'Angelo, A, Delille, B, Fer, I, Fong, AA, Fransson, A, Fuchs, N, Gardner, J, Granskog, MA, Hoppe, CJM, Hoppe, M, Hoppmann, M, Mock, T, Muller, S, Müller, O, Nicolaus, M, Nomura, D, Petäjä, T, Salganik, E, Schmale, J, Schmidt, K, Schulz, KM, Shupe, MD, Stefels, J, Thielke, L, Tippenhauer, S, Ulfso, A, van Leeuwe, M, Webster, M, Yoshimura, M, Zhan, L. 2023. Thin and transient meltwater layers and false bottoms in the Arctic sea ice

pack—Recent insights on these historically overlooked features. *Elementa: Science of the Anthropocene* **11**(1): 00025. DOI: <https://dx.doi.org/10.1525/elementa.2023.00025>.

Smith, MM, von Albedyll, L, Raphael, IA, Lange, BA, Matero, I, Salganik, E, Webster, MA, Granskog, MA, Fong, A, Lei, R, Light, B. 2022. Quantifying false bottoms and under-ice meltwater layers beneath Arctic summer sea ice with fine-scale observations. *Elementa: Science of the Anthropocene* **10**(1): 000116. DOI: <https://dx.doi.org/10.1525/elementa.2021.000116>.

Snoeijs-Leijonmalm, P, Flores, H, Sakinan, S, Hildebrandt, N, Svenson, A, Castellani, G, Vane, K, Mark, FC, Heuzé, C, Tippenhauer, S, Niehoff, B, Hjelm, J, Sundberg, JH, Schaafsma, FL, Engelmann, R, The EFICA-MOSAiC Team. 2022. Unexpected fish and squid in the central Arctic deep scattering layer. *Science Advances* **8**(7): eabj7536. DOI: <https://dx.doi.org/10.1126/sciadv.abj7536>.

Somavilla, R, Schauer, U, Budéus, G. 2013. Increasing amount of Arctic Ocean deep waters in the Greenland Sea. *Geophysical Research Letters* **40**(16): 4361–4366. DOI: <https://dx.doi.org/10.1002/grl.50775>.

Son, EY, Kawaguchi, Y, Cole, ST, Toole, JM, Ha, HK. 2022. Assessment of turbulent mixing associated with eddy-wave coupling based on autonomous observations from the Arctic Canada Basin. *Journal of Geophysical Research: Oceans* **127**(9): e2022JC018489. DOI: <https://dx.doi.org/10.1029/2022JC018489>.

Stanton, T, Shaw, B. 2023. Observations from Autonomous Ocean Flux Buoy 45 deployed at site L3 during the MOSAiC transpolar drift, Arctic Basin, 2019–2020. Arctic Data Center. DOI: <https://dx.doi.org/10.18739/A26W96B3T>.

Stanton, TP, Shaw, WJ, Hutchings, JK. 2012. Observational study of relationships between incoming radiation, open water fraction, and ocean-to-ice heat flux in the Transpolar Drift: 2002–2010. *Journal of Geophysical Research: Oceans* **117**(C7). DOI: <https://dx.doi.org/10.1029/2011JC007871>.

Stedmon, CA, Amon, RMW, Bauch, D, Bracher, A, Gonçalves-Araujo, R, Hoppmann, M, Krishfield, RA, Laney, S, Rabe, B, Reader, HE, Granskog, MA. 2021a. Intercalibrated dataset of in situ dissolved organic matter fluorescence collected using ice tethered profilers in the Central Arctic (2011–2016). PANGAEA. DOI: <https://dx.doi.org/10.1594/PANGAEA.934370>.

Stedmon, CA, Amon, RMW, Bauch, D, Bracher, A, Gonçalves-Araujo, R, Hoppmann, M, Krishfield, R, Laney, S, Rabe, B, Reader, H, Granskog, MA. 2021b. Insights into water mass origins in the central Arctic Ocean from in-situ dissolved organic matter fluorescence. *Journal of Geophysical Research: Oceans* **126**(7): e2021JC017407. DOI: <https://dx.doi.org/10.1029/2021JC017407>.

Steele, M, Boyd, T. 1998. Retreat of the cold halocline layer in the Arctic Ocean. *Journal of Geophysical Research: Oceans* **103**(C5): 10419–10435. DOI: <https://dx.doi.org/10.1029/98JC00580>.

Steele, M, Morison, J, Ermold, W, Rigor, I, Ortmeyer, M, Shimada, K. 2004. Circulation of summer Pacific halocline water in the Arctic Ocean. *Journal of Geophysical Research: Oceans* **109**(C2). DOI: <https://dx.doi.org/10.1029/2003JC002009>.

Steele, M, Morley, R, Ermold, W. 2001. PHC3 updated from: A global ocean hydrography with a high quality Arctic Ocean. *Journal of Climate* **14**(9): 2079–2087. DOI: [https://doi.org/10.1175/1520-0442\(2001\)014<2079:PAGOHW>2.0.CO;2](https://doi.org/10.1175/1520-0442(2001)014<2079:PAGOHW>2.0.CO;2).

Stroeve, J, Serreze, M, Drobot, S, Gearheard, S, Holland, M, Maslanik, J, Meier, W, Scambos, T. 2008. Arctic sea ice extent plummets in 2007. *Eos, Transactions American Geophysical Union* **89**(2): 13–14. DOI: <https://dx.doi.org/10.1029/2008EO020001>.

Takahashi, T, Sutherland, SC, Wanninkhof, R, Sweeney, C, Feely, RA, Chipman, DW, Hales, B, Friederich, G, Chavez, F, Sabine, C, Watson, A, Bakker, DCE, Schuster, U, Metzl, N, Yoshikawa-Inoue, H, Ishii, M, Midorikawa, T, Nojiri, Y, Körtzinger, A, Steinhoff, T, Hoppema, M, Olafsson, J, Arnarson, TS, Tilbrook, B, Johannessen, T, Olsen, A, Bellerby, R, Wong, CS, Delille, B, Bates, NR, de Baar, HJW. 2009. Climatological mean and decadal change in surface ocean pCO₂, and net sea–air CO₂ flux over the global oceans. *Deep Sea Research Part II: Topical Studies in Oceanography* **56**(8–10): 554–577. DOI: <https://dx.doi.org/10.1016/j.dsr2.2008.12.009>.

Tanhua, T, Jones, EP, Jeansson, E, Jutterström, S, Smethie Jr, WM, Wallace, DW, Anderson, LG. 2009. Ventilation of the Arctic Ocean: Mean ages and inventories of anthropogenic CO₂ and CFC-11. *Journal of Geophysical Research: Oceans* **114**(C1). DOI: <https://dx.doi.org/10.1029/2008JC004868>.

Terhaar, J, Lauerwald, R, Regnier, P, Gruber, N, Bopp, L. 2021. Around one third of current Arctic Ocean primary production sustained by rivers and coastal erosion. *Nature Communications* **12**(1): 169. DOI: <https://dx.doi.org/10.1038/s41467-020-20470-z>.

Timmermans, M-L, Marshall, J. 2020. Understanding Arctic Ocean circulation: A review of ocean dynamics in a changing climate. *Journal of Geophysical Research: Oceans* **125**(4): e2018JC014378. DOI: <https://dx.doi.org/10.1029/2018JC014378>.

Timmermans, M-L, Toole, JM. 2023. The Arctic Ocean's Beaufort Gyre. *Annual Review of Marine Science* **15**: 223–248. DOI: <https://dx.doi.org/10.1146/annurev-marine-032122-012034>.

Tippenhauer, S, Janout, M, Chouksey, M, Torres-Valdes, S, Fong, A, Wulff, T. 2021. Substantial sub-surface chlorophyll patch sustained by vertical nutrient fluxes in Fram Strait observed with an autonomous underwater vehicle. *Frontiers in Marine Science* **8**: 605225. DOI: <https://dx.doi.org/10.3389/fmars.2021.605225>.

Tippenhauer, S, Vredenborg, M, Heuzé, C, Ulfsbo, A, Rabe, B, Granskog, MA, Allerholt, J, Balmonte, JP, Campbell, RG, Castellani, G, Chamberlain, E, Creamean, J, D'Angelo, A, Dietrich, U, Droste, E, Eggers, L, Fang, YC, Fong, AA, Gardner, J, Downloaded from <http://online.ucpress.edu/elementa/article-pdf/12/1/00114/828492/elementa.2023.00114.pdf> by guest on 05 September 2024

Graupner, R, Grosse, J, He, H, Hildebrandt, N, Hoppe, CJM, Hoppmann, M, Kanzow, T, Karam, S, Koenig, Z, Kong, B, Kuhlmeiy, D, Kuznetsov, I, Lan, M, Liu, H, Mallet, M, Mohrholz, V, Muilwijk, M, Müller, O, Olsen, LM, Rember, R, Ren, J, Sakinan, S, Schaffer, J, Schmidt, K, Schuffenhauer, I, Schulz, K, Shoemaker, K, Spahic, S, Sukhikh, N, Svenson, A, Torres-Valdés, S, Torstensson, A, Wischnewski, L, Zhuang, Y. 2023a. Physical oceanography based on Ocean City CTD during POLARSTERN cruise PS122. PANGAEA. DOI: <https://doi.pangaea.de/10.1594/PANGAEA.959964>.

Tippenhauer, S, Vredenborg, M, Heuzé, C, Ulfsbo, A, Rabe, B, Granskog, MA, Allerholt, J, Balmonte, JP, Campbell, RG, Castellani, G, Chamberlain, E, Creamean, J, D'Angelo, A, Dietrich, U, Droste, E, Eggers, L, Fang, YC, Fong, AA, Gardner, J, Graupner, R, Grosse, J, He, H, Hildebrandt, N, Hoppe, CJM, Hoppmann, M, Kanzow, T, Karam, S, Koenig, Z, Kong, B, Kuhlmeiy, D, Kuznetsov, I, Lan, M, Liu, H, Mallet, M, Mohrholz, V, Muilwijk, M, Müller, O, Olsen, LM, Rember, R, Ren, J, Sakinan, S, Schaffer, J, Schmidt, K, Schuffenhauer, I, Schulz, K, Shoemaker, K, Spahic, S, Sukhikh, N, Svenson, A, Torres-Valdés, S, Torstensson, A, Wischnewski, L, Zhuang, Y. 2023b. Physical oceanography based on ship CTD during POLARSTERN cruise PS122. PANGAEA. DOI: <https://doi.pangaea.de/10.1594/PANGAEA.959963>.

Tippenhauer, S, Vredenborg, M, Heuzé, C, Ulfsbo, A, Rabe, B, Granskog, MA, Allerholt, J, Balmonte, JP, Campbell, RG, Castellani, G, Chamberlain, E, Creamean, J, D'Angelo, A, Dietrich, U, Droste, E, Eggers, L, Fang, YC, Fong, AA, Gardner, J, Graupner, R, Grosse, J, He, H, Hildebrandt, N, Hoppe, CJM, Hoppmann, M, Kanzow, T, Karam, S, Koenig, Z, Kong, B, Kuhlmeiy, D, Kuznetsov, I, Lan, M, Liu, H, Mallet, M, Mohrholz, V, Muilwijk, M, Müller, O, Olsen, LM, Rember, R, Ren, J, Sakinan, S, Schaffer, J, Schmidt, K, Schuffenhauer, I, Schulz, K, Shoemaker, K, Spahic, S, Sukhikh, N, Svenson, A, Torres-Valdés, S, Torstensson, A, Wischnewski, L, Zhuang, Y. 2023c. Physical oceanography water bottle samples based on ship CTD during POLARSTERN cruise PS122. PANGAEA. DOI: <https://doi.pangaea.de/10.1594/PANGAEA.959965>.

Tippenhauer, S, Vredenborg, M, Heuzé, C, Ulfsbo, A, Rabe, B, Granskog, MA, Allerholt, J, Balmonte, JP, Campbell, RG, Castellani, G, Chamberlain, E, Creamean, J, D'Angelo, A, Dietrich, U, Droste, E, Eggers, L, Fang, YC, Fong, AA, Gardner, J, Graupner, R, Grosse, J, He, H, Hildebrandt, N, Hoppe, CJM, Hoppmann, M, Kanzow, T, Karam, S, Koenig, Z, Kong, B, Kuhlmeiy, D, Kuznetsov, I, Lan, M, Liu, H, Mallet, M, Mohrholz, V, Muilwijk, M, Müller, O, Olsen, LM, Rember, R, Ren, J, Sakinan, S, Schaffer, J, Schmidt, K, Schuffenhauer, I, Schulz, K, Shoemaker, K, Spahic, S, Sukhikh, N, Svenson, A, Torres-Valdés, S, Torstensson, A, Wischnewski, L, Zhuang, Y. 2023d. Physical oceanography water bottle samples based on Ocean City CTD during POLARSTERN cruise PS122. PANGAEA. DOI: <https://doi.pangaea.de/10.1594/PANGAEA.959966>.

Toole, JM, Krishfield, R, Woods Hole Oceanographic Institution Ice-Tethered Profiler Program. 2016. Ice-Tethered Profiler observations: Vertical profiles of temperature, salinity, oxygen, and ocean velocity from an Ice-Tethered Profiler buoy system. [ITP94, ITP111, accessed March 13, 2023]. NOAA National Centers for Environmental Information. DOI: <https://dx.doi.org/10.7289/v5mw2f7x>.

Toole, JM, Krishfield, RA, Timmermans, ML, Proshutinsky, A. 2011. The ice-tethered profiler: Argo of the Arctic. *Oceanography* **24**(3): 126–135. DOI: <https://dx.doi.org/10.5670/oceanog.2011.64>.

Torres-Valdés, S, Tsubouchi, T, Bacon, S, Naveira-Garabato, AC, Sanders, R, McLaughlin, FA, Petrie, B, Kattner, G, Azetsu-Scott, K, Whitledge, TE. 2013. Export of nutrients from the Arctic Ocean. *Journal of Geophysical Research: Oceans* **118**(4): 1625–1644. DOI: <https://dx.doi.org/10.1002/jgrc.20063>.

von Appen, W-J, Baumann, TM, Janout, M, Koldunov, N, Lenn, Y-D, Pickart, RS, Scott, RB, Wang, Q. 2022. Eddies and the distribution of eddy kinetic energy in the Arctic Ocean. *Oceanography* **35**(3/4): 42–51. Available at <https://www.jstor.org/stable/27182695>.

von Appen, W-J, Schauer, U, Somavilla, R, Bauerfeind, E, Beszczynska-Möller, A. 2015. Exchange of warming deep waters across Fram Strait. *Deep Sea Research Part I: Oceanographic Research Papers* **103**: 86–100. DOI: <https://dx.doi.org/10.1016/j.dsr.2015.06.003>.

Wang, Q, Shu, Q, Bozec, A, Chassignet, EP, Fogli, PG, Fox-Kemper, B, Hogg, AM, Iovino, D, Kiss, AE, Koldunov, N, Le Sommer, J, Li, Y, Lin, P, Liu, H, Polyakov, I, Scholz, P, Sidorenko, D, Wang, S, Xu, X. 2023. Impact of high resolution on Arctic Ocean simulations in Ocean Model Intercomparison Project phase 2 (OMIP-2). *Geoscientific Model Development Discussions* **2023**: 1–46. DOI: <https://dx.doi.org/10.5194/gmd-2023-123>.

Webster, MA, Holland, M, Wright, NC, Hendricks, S, Hutter, N, Itkin, P, Light, B, Linhardt, F, Perovich, DK, Raphael, IA, Smith, MM, von Albedyll, L, Zhang, J. 2022. Spatiotemporal evolution of melt ponds on Arctic sea ice: MOSAiC observations and model results. *Elementa: Science of the Anthropocene* **10**(1): 000072. DOI: <https://dx.doi.org/10.1525/elementa.2021.000072>.

Zhao, M, Timmermans, M-L, Cole, S, Krishfield, R, Proshutinsky, A, Toole, J. 2014. Characterizing the eddy field in the Arctic Ocean halocline. *Journal of Geophysical Research: Oceans* **119**(12): 8800–8817. DOI: <https://dx.doi.org/10.1002/2014JC010488>.

Zweng, M, Reagan, J, Seidov, D, Boyer, T, Locarnini, R, Garcia, H, Mishonov, A, Baranova, O, Weathers, K, Paver, C, Smolyar, I. 2018. World Ocean Atlas 2018, Volume 2: Salinity. A. Mishonov Technical Ed.; NOAA Atlas NESDIS 82. Available at <http://www.nodc.noaa.gov/OC5/indprod.html>. Accessed March 30, 2023.

How to cite this article: Schulz, K, Koenig, Z, Muilwijk, M, Bauch, D, Hoppe, CJM, Droste, ES, Hoppmann, M, Chamberlain, EJ, Laukert, G, Stanton, T, Quintanilla-Zurita, A, Fer, I, Heuzé, C, Karam, S, Mieruch-Schnüller, S, Baumann, TM, Vredenborg, M, Tippenhauer, S, Granskog, MA. 2024. The Eurasian Arctic Ocean along the MOSAiC drift in 2019–2020: An interdisciplinary perspective on physical properties and processes. *Elementa: Science of the Anthropocene* 12(1). DOI: <https://doi.org/10.1525/elementa.2023.00114>

Domain Editor-in-Chief: Jody W. Deming, University of Washington, Seattle, WA, USA

Associate Editor: Mathieu Ardyna, Stanford University, Stanford, CA, USA

Knowledge Domain: Ocean Science

Part of an Elementa Special Feature: The Multidisciplinary Drifting Observatory for the Study of Arctic Climate (MOSAiC)

Published: July 05, 2024 **Accepted:** May 13, 2024 **Submitted:** September 03, 2023

Copyright: © 2024 The Author(s). This is an open-access article distributed under the terms of the Creative Commons Attribution 4.0 International License (CC-BY 4.0), which permits unrestricted use, distribution, and reproduction in any medium, provided the original author and source are credited. See <http://creativecommons.org/licenses/by/4.0/>.



Elem Sci Anth is a peer-reviewed open access journal published by University of California Press.

OPEN ACCESS 